



34 volatile organic compounds (VOCs) appear to play a minor role in the initial cluster formation but  
35 contribute significantly to the consecutive growth process. Regarding alkaline molecules, amines, are  
36 insufficient to stabilize all sulfuric acid clusters in Po Valley. Ion cluster measurements and kinetic  
37 models suggest that ammonia (10 ppb) must therefore also play a role in the nucleation process.  
38 Generally, the high formation rates of sub-2 nm particles ( $87 \text{ cm}^{-3} \text{ s}^{-1}$ ) and nucleation mode growth rates  
39 ( $5.1 \text{ nm h}^{-1}$ ) together with the relatively low condensational sink ( $8.9 \times 10^{-3} \text{ s}^{-1}$ ) will result in a high  
40 survival probability of newly formed particles, making NPF crucial for the springtime aerosol number  
41 budget. Our results also indicate that reducing key pollutants such as  $\text{SO}_2$ , amine and  $\text{NH}_3$ , could help  
42 to decrease the particle number concentrations substantially in the Po Valley region.

## 43 **1. Introduction**

44 New particle formation (NPF) occurs ubiquitously in the troposphere and affects the global climate  
45 (Dunne et al., 2016) and local or regional air quality (Kulmala et al., 2021). NPF and further growth of  
46 the newly formed particles dominate aerosol number concentrations and are the major contributor to  
47 the ultrafine (<100 nm) aerosol budget, which poses a significant health threat to the population in  
48 polluted areas (Schraufnagel, 2020). While air pollution mitigation strategies mostly focus on reducing  
49 particulate mass (particulate matter below  $2.5 \mu\text{m}$  ( $\text{PM}_{2.5}$ )), ultrafine particle number concentrations  
50 might not be affected by such policies (De Jesus et al., 2019). It is therefore essential that we understand  
51 the mechanisms leading to NPF in polluted environments to design better targeted air quality strategies  
52 for polluted European regions, where  $\text{PM}_{2.5}$  reduction measures are already implemented.

53 NPF is closely linked to atmospheric air pollution. Efficient nucleation and growth are crucial factors  
54 contributing to haze formation, according for over 65% of the particle number concentrations in urban  
55 environment (Kulmala et al., 2021; Guo et al., 2014). Frequent NPF events have also been observed in  
56 heavily polluted urban environments, including megacities in China (Chu et al., 2019; Yao et al., 2018;  
57 Du et al., 2022) and India (Sebastian et al., 2022). Strong and frequent NPF events have been reported  
58 in the most urbanization areas in China, such as the North China Plain (Wang et al., 2015; Wang et al.,  
59 2013; Wu et al., 2011; Wu et al., 2007; Shen et al., 2011), Yangtze River Delta (Dai et al., 2017; Yu et  
60 al., 2016; Xiao et al., 2015) and Peal River Delta (Yue et al., 2013; Peng et al., 2014; Liu et al., 2008).  
61 This observation contradicts theoretical calculations that suggest NPF events are less likely to occur in  
62 polluted areas, where high levels of preexisting aerosols acting as condensational sinks (CS) are capable  
63 of quickly scavenging gaseous precursors of NPF (Kulmala et al., 2017).

64 The elucidation of NPF precursors and mechanisms has varied among different sampling locations and  
65 studies. No uniform theory or mechanism can elucidate the NPF occurrence in different polluted areas  
66 or in different seasons. For example, in Shanghai and Beijing, China, sulfuric acid (SA,  $\text{H}_2\text{SO}_4$ ) and  
67 amines were identified as key contributors to initial particle formations (Yao et al., 2018; Cai et al.,  
68 2021; Yan et al., 2021). On the other hand, some studies also suggests that photooxidation products of  
69 vehicle emitted organic vapors, dominate NPF in urban conditions rather than SA or base species (Guo  
70 et al., 2020). Meanwhile, in Barcelona, Spain, which is significantly less polluted than Asian megacities  
71 but still shows frequent high pollution levels, NPF was reported to be associated with SA along with  
72 highly oxygenated organic molecules (HOMs) (Brean et al., 2020). The discrepancies in the reported  
73 NPF mechanisms may arise from the limited utilization of state-of-the-art instruments, such as those  
74 capable of measuring size distribution down to 1-2 nm and directly identifying clusters and vapors with  
75 the influences by spatio-temporal variations (Wang et al., 2017). Therefore, gaining a better knowledge  
76 of the key participants, nucleation mechanism and the roles of pre-existing particles is crucial for  
77 comprehending the causes of the high NPF frequencies in polluted regions. This knowledge can be  
78 essential for developing effective local  $\text{PM}_{2.5}$  control and implementation strategies.

79 The Po Valley region is one of the most important industrial and agricultural areas in Southern Europe  
80 with dense population ( $>17$  million/ $70,000 \text{ km}^2$ ). It is located in northern Italy, surrounded by the Alps  
81 (in the north), the Apennine mountains (in the south), and the Adriatic Sea (in the east). High primary  
82 anthropogenic emissions, a mixture of numerous pollutants from industrial, urban and agricultural

83 sources, together with frequently occurring stagnant meteorological conditions in winter make the Po  
84 Valley region a hotspot in Europe for high aerosol loadings (Saarikoski et al., 2012; Li et al., 2014;  
85 Finzi and Tebaldi, 1982; Daellenbach et al., 2023). But it is distinct from Asian megacities as the  
86 population density is significantly lower (250 people km<sup>-2</sup> in Po Valley compared to e.g., 1 400 people  
87 km<sup>-2</sup> in Beijing), resulting in effects such as traffic or residential heating being less dominant pollution  
88 sources. At the same time, NPF occurs frequently in the Po Valley (Hamed et al., 2007; Manninen et  
89 al., 2010). For example, Shen et al. (2021) observed that NPF events took place on approximately 70%  
90 of the days during spring and summer. Similarly, Kontkanen et al. (2017) discovered that during  
91 summer, NPF occurred on 89% of the days. During NPF event days, high formation rates of sub-2nm  
92 neutral particles ( $J_2$ ,  $\sim 10^1$  to  $10^2$  cm<sup>-3</sup> s<sup>-1</sup>, (Kontkanen et al., 2017)) and SA concentrations ( $\sim 1 \times 10^7$  cm<sup>-3</sup>)  
93 were observed in the Po Valley (Paasonen et al., 2010; Kontkanen et al., 2017). These levels were  
94 among the highest recorded in a study conducted at nine sites across the Northern Hemisphere  
95 (Kontkanen et al., 2017).

96 While previous studies conducted in the Po Valley have reported frequent NPF events characterized by  
97 high nucleation and growth rates, the clustering mechanism and the dominant precursors for particle  
98 growth have not been investigated to-date. Especially with respect to the distinct features of Po-Valley  
99 compared to the more intensely researched megacity environments, a deeper understanding of frequent  
100 NPF events, including their precursors, nucleation mechanisms, and growth processes is crucial for air  
101 pollution control and the effective implementation of PM<sub>2.5</sub> mitigation measures in such semi-urban but  
102 highly industrialized regions as Po Valley. In this study, we conducted a 2-month field campaign in the  
103 months of March – April 2022, we 1) identified the chemical composition of atmospheric neutral and  
104 ion clusters by a set of state-of-the-art mass spectrometers, 2) characterized the initial NPF and further  
105 growth rates using particle number size distribution measurement down to 1 nm, and 3) compared the  
106 field measurement results with the recent Cosmics Leaving Outdoor Droplets (CLOUD) chamber  
107 experiments to investigate the mechanism of NPF events in the Po Valley region. This allowed us to  
108 elucidate the NPF and growth mechanisms at a severely polluted Southern European site, and to give  
109 insights in best mitigation strategies for ultrafine particle pollution in the context of already  
110 implemented PM<sub>2.5</sub> reduction strategies.

## 111 2. Method

### 112 2.1 Measurement site

113 Our measurement was part of the Fog and Aerosol InterRAction Research Italy (FAIRARI) field  
114 campaign in San Pietro Capofiume (SPC, 44.65°N, 11.62°E, 5 m a.s.l.), located in the Po Valley region  
115 in Northern Italy. The measurement site is part of the Aerosol, Clouds and Trace Gases Research  
116 Infrastructure (ACTRIS)-Italy network and operated by the Italian National Research Council-Institute  
117 of Atmospheric Sciences and Climate (CNR-ISAC). The SPC site is approximately 30 km northeast of  
118 Bologna (~400, 000 residents) and 20 km south of Ferrara (~130, 000 residents), the two major cities  
119 in the area. The distance from the measurement site to the Adriatic Sea (to the east) is about 50 km. The  
120 area around the sampling site consists of agricultural fields and a smaller town (<2, 000 inhabitants,  
121 within 5 km) and smaller settlements in the proximity. Given its location, the SPC rural station is  
122 considered to be representative of the regional background of the Po Valley (Paglione et al., 2021;  
123 Paasonen et al., 2010; Hamed et al., 2007; Saarikoski et al., 2012; Decesari et al., 2014; Paglione et al.,  
124 2020). The instruments for the NPF measurement were operated in a temperature controlled ( $\sim 20$  °C)  
125 container from March 1 to April 30, 2022.

126 During the sampling period, the daily average temperature ranged from 1°C to 17°C. The average wind  
127 speed (WS) was approximately  $2.4 \pm 1.5$  m/s (Fig. 1b). The average WS in the daytime was 3.5 m/s from  
128 the east, which was significantly higher than at night (1.5 m/s) from the west. Strong diurnal variations  
129 of wind direction were observed, which was typically from the west at night and shifted to the east  
130 during the day (Fig. 1a). This pattern was potentially influenced by the sea-land breeze from the Adriatic  
131 Sea. Accordingly, the daily average relative humidity (RH) varied from 41% to 98%, with values as

132 high as 85% at night, which sharply decreased to around 40% at noon caused by the strong temperature  
133 variation.

## 134 **2.2 Instruments**

### 135 **2.2.1 Chemical composition measurements**

136 The chemical composition of cluster ions was measured using a high-resolution atmospheric-pressure-  
137 interface time-of-flight mass spectrometer (APi-TOF, Aerodyne Research Inc. & Tofwerk AG). The  
138 APi-TOF measures naturally charged ions present in the ambient environment. A detailed description  
139 of the instrument can be found in Junninen et al. (2010). In this study, ambient air was sampled through  
140 a 0.57-meter stainless steel tube with a flow rate of ~10 liters per minute (LPM), with 0.8 LPM of the  
141 sample flow entering the APi-TOF.

142 The concentration of SA was measured using a nitrate ion ( $\text{NO}_3^-$ )-based chemical-ionization (CI)  
143 atmospheric-pressure-interface time-of-flight mass spectrometer (CI-APi-TOF, Aerodyne Research Inc.  
144 & Tofwerk AG (Jokinen et al., 2012)). The CI-APi-TOF is an APi-TOF coupled with a CI-unit,  
145 equipped with a soft X-ray source (L9490, Hamamatsu's 9.5 kV) to produce the primary ions. The  
146 sampling flow went into the instrument through a ~0.6-meter  $\frac{3}{4}$  inch stainless steel tube. The sampling  
147 flow was 10 LPM and the sheath flow was set to 20 LPM. Data acquisitions for CI-APi-TOF was  
148 performed with a time resolution of 10 s. A calibration factor of  $1.0 \times 10^{10} \text{ cm}^{-3}$  for SA was determined  
149 with sampling loss corrections before the campaign according to the method proposed by Kurten et al.  
150 (2012).

151 Dimethylamine (DMA) measurements were performed using a Vocus CI-ToF (time-of-flight) mass  
152 spectrometer (hereafter Vocus, Aerodyne Research Inc. & Tofwerk AG) using  $\text{H}_3\text{O}^+$  as a reagent ion.  
153 The Vocus has been described in detail in Krechmer et al. (2018) and the study by Wang et al. (2020)  
154 utilized Vocus for DMA observations. In this study, the Focusing Ion-Molecular Reactor (FIMR) of  
155 Vocus operated at a pressure of 2.0 mbar and a temperature of 100 °C with the radio frequency  
156 amplitude of 350 V and frequency of  $1.4 \times 10^6$  Hz. Data acquisition was performed with a time  
157 resolution of 10 s in the mass range 0 –1000 amu.

### 158 **2.2.2 Particle size distribution measurements**

#### 159 **Particle Size Magnifier**

160 The Airmodus A11 nano-CNC-system (nano-Condensation Nucleus Counter), colloquially known as  
161 the Particle Size Magnifier (PSM) is a two-step condensation particle counter (CPC) capable of  
162 measuring particle size distributions of sub-3nm particles (Vanhanen et al., 2011). The system consists  
163 of two parts, in which the PSM (Airmodus A10) acts as a preconditioner where particles are grown first  
164 before being funneled to the CPC (Airmodus A20) for further growth and optical detection. In the PSM  
165 the sample flow is turbulently mixed with a heated flow saturated with diethylene glycol (DEG) in the  
166 mixing section and the DEG then condenses on the particles in the growth tube. By scanning the flow  
167 rate through the DEG saturator, the smallest activated particle size is altered which can be converted  
168 into a sub-3nm particle size distribution. Further particle growth is achieved by butanol in the CPC such  
169 that the particles reach optically detectable sizes.

170 The PSM was calibrated according to the standard operation procedure for PSM (Lehtipalo et al., 2022)  
171 using a known aerosol population from a glowing tungsten wire generator (Kangasluoma et al., 2015;  
172 Peineke et al., 2006). The detection efficiency for different particle sizes was determined by comparing  
173 the concentration of size selected particles to a reference instrument, in this case a Faraday cup  
174 electrometer.

175 The system was set up with an Airmodus Nanoparticle Diluter (AND) inlet (Lampimäki et al., 2023)  
176 for sample dilution and automatic background measurement to make sure that the CPC stays within a  
177 single counting range during the campaign. The inlet was set up at around 2 meters above the ground

178 and the background was measured roughly every 8 hours and subtracted from the signal during the  
179 inversion process.

## 180 **HFDMPs and Hauke-type DMPS**

181 The high-flow differential mobility particle sizer (HFDMPs) system utilizes a half-mini differential  
182 mobility analyzer (DMA, (Fernández De La Mora and Kozlowski, 2013; Cai et al., 2018)) to size-select  
183 particles that are then grown and detected by an A11 nano Condensation Nucleus Counter system  
184 (Airmodus Ltd., A11 nano-CNC) (Kangasluoma et al., 2018). The HFDMPs significantly improves  
185 sub-10 nm particle measurements compared to a typical differential mobility particle sizer (DMPS)  
186 system, allowing us to better characterize the sub-10 nm particle size distribution when combined with  
187 the PSM measurements. The DMA was size-calibrated with electro sprayed positively charged  
188 monomer ions of tetraethylammonium bromide (THA<sup>+</sup>) (Ude and De La Mora, 2005).

189 The HFDMPs inlet was set up at a height of 1 m and used a 50 cm long 10 mm outer diameter tube  
190 with a core sampling system to minimize losses (Kangasluoma et al., 2016; Fu et al., 2019). A home-  
191 built Soft X-Ray ionization source (similar to the TSI Inc. Model 3087) was used to charge particles.  
192 The HFDMPs measured the particle size-distribution from 2–15 nm for both polarities at 15 predefined  
193 size-steps within 10 minutes.

194 Sampling from the same inlet and using the same charging device, a conventional DMPS system  
195 equipped with a Hauke-type DMA (aerosol flow 1 LPM, sheath flow 5 LPM) and a TSI Inc. CPC  
196 (Model 3772) was measuring the particle size-distribution from 10–800 nm at 16 predefined size-steps  
197 within 10 minutes. In addition, a DMPS measuring from 15–800 nm was available in another  
198 measurement container at the same field site. The total particle number concentrations obtained from  
199 integrating the particle size-distribution measured by the DMPS was compared with a reference CPC  
200 (TSI Inc. Model 3025A) operated at the same site during the first weeks of the campaign. It revealed  
201 on average a factor of 2 lower concentrations measured by the Hauke-type DMPS which was confirmed  
202 to be rather size-independent by a comparison of the measured size-distributions and their overlap with  
203 the HF-DMPS system and was thus subsequently corrected for.

### 204 **2.2.3 Co-located measurements**

205 Additional co-located measurements of auxiliary data from CNR-ISAC network ([www.isac.cnr.it/en](http://www.isac.cnr.it/en))  
206 and from the routine monitoring program of the Regional environmental protection agency of Emilia  
207 Romagna (ARPAE, <https://www.arpae.it/it>) were used in this study. An online High-Resolution Time-  
208 of-Flight Aerosol Mass Spectrometer (HR-ToF-AMS, Aerodyne Research) and a Multi Angle  
209 Absorption Photometer (MAAP, Thermo Scientific) were operated on the same site for the  
210 measurement of non-refractory species and black carbon (BC), respectively. Trace gases were also  
211 measured with 1 minute time resolution: O<sub>3</sub> (Thermo Scientific, model TEI-49i), NO<sub>x</sub> (Teledyne-API,  
212 model 200A), NH<sub>3</sub> (Teledyne-API, model 201E), and SO<sub>2</sub> (Thermo Scientific, Model 43i Trace Level-  
213 Enhanced). Moreover, meteorological parameters (e.g., RH, temperature, wind direction and wind  
214 speed) were measured by a meteorology station (VAISALA Ltd, model wxt536).

215

## 216 **2.3 Data processing**

### 217 **2.3.1 New particle formation classification**

218 We classified each day according to whether a growing mode appeared in the particle size distribution  
219 or not. This classification was done separately for both the HFDMPs and the PSM size distributions. A  
220 growing mode was defined as a new particle mode that appeared in the particle size distribution and  
221 continued to grow to larger sizes for at least two hours. If there was a growing mode visible in both the  
222 PSM and HFDMPs size distributions, the day was defined as "NPF with growth". If there was no  
223 growth or the growth was unclear in the HFDMPs size distribution but there was a growing mode in  
224 the PSM size distribution, then the day was classified as "NPF with no growth". If there was no growing  
225 mode in either size distribution, then the day was marked as "no NPF events". The definition is similar  
226 to Dada et al. (2018) who used naturally charged ions to separate between NPF days with clustering

227 only and clustering plus visible growth. If there was a growing or an undefined new mode visible in the  
228 combined size distribution but there was no clustering detected by the PSM, this day was marked as  
229 "unclear". Days that lacked data from one of the instruments were marked as "no data".

### 230 2.3.2 Condensation sink, nucleation and growth rate calculations

231 The condensation sink and coagulation sink were calculated according to Dal Maso et al. (2005) from  
232 the Hauke-type DMPS size distribution without any correction of aerosol hygroscopic behavior. Growth  
233 rates were calculated using the maximum concentration method, in which we fit a Gaussian distribution  
234 to the particle concentration evolution at a fixed size to determine the time of maximum concentration  
235 for a given size channel in the HFDMPs.

236 The growth rates were calculated by first determining the time to reach 50% of the maximum  
237 concentration and then the average growth rate is derived as the slope of the linear fit between the time  
238 and diameter:

$$239 \quad GR = \frac{\Delta d_p}{\Delta t} \approx \frac{d_{p,f} - d_{p,i}}{t_f - t_i}, \quad (1)$$

240 where  $d_{p,f}$  is the diameter at the end time  $t_f$  and  $d_{p,i}$  is the diameter at the start time  $t_i$ .

241 From these, the growth rate was calculated as the slope of a linear least squares fit to the time-points of  
242 maximum concentration and their corresponding particle diameters. The formation rates were  
243 calculated for several sizes by using the balance equation in Kulmala et al. (2012) using the combined  
244 DMPS size-distributions ( $J_2$ ,  $J_3$ ,  $J_6$ ) and the PSM plus combined DMPS size-distribution ( $J_{1.7}$ ).  
245 Formation rates were then calculated by rearranging the equation describing the time evolution of the  
246 particle size distribution. Formation rate for a given diameter  $d_{p1}$  is calculated as

$$247 \quad J_{dp1} = \frac{dN_{dp1-dp2}}{dt} + CoagS_{dp1} \cdot N_{dp1-dp2} + \frac{GR}{\Delta d_p} N_{dp1-dp2}, \quad (2)$$

248

### 249 2.3.3 Mass spectrometer data analysis

250 The APi-TOF and CI-APi-TOF data were analyzed using the Tofware package (v.3.1.0, Tofwerk,  
251 Switzerland, and Aerodyne, USA) in the Igor Pro software (v.7.08, WaveMetrics, USA). The mass  
252 accuracy is within 10 ppm (APi-TOF) and 5 ppm (CI-APi-TOF), and the mass resolutions were ~4500  
253 (APi-TOF) and ~5000 (CI-APi-TOF) for ions >200 Th. The raw signals were firstly normalized by the  
254 primary ions ( $\text{NO}_3^-$ , monomer, dimer and trimer) and then multiplied by the calibration factor of SA.  
255 Detailed information on the mass spectrometer data analysis methods can be found in previous studies  
256 (Cai et al., 2022; Cai et al., 2023a; Zha et al., 2018; Zha et al., 2023a; Fan et al., 2021; Zha et al., 2023b).

### 257 2.3.4 Kinetic model Simulations

258 In order to evaluate the contribution of SA-amine clustering to cluster formation in the Po Valley, we  
259 applied a kinetic model to simulate SA dimer concentrations. We simulated the cluster concentrations  
260 and particle formation rates under different amine levels based on the model. The simulation was  
261 performed with a temperature of 283 K, atmospheric pressure of  $1.01 \times 10^5$  Pa, and the condensation  
262 sink (CS) of  $0.01 \text{ s}^{-1}$  based on our measurement during the sampling period. In the model, the formation  
263 rate of SA tetramer was regarded as the simulated particle formation rate. The standard molar Gibbs  
264 free energy of formation and the corresponding evaporation of SA-amine clusters was based on  
265 quantum chemistry with corrections from the experimental data. The detailed settings of the kinetic  
266 model can be found in Cai et al. (2021).

## 267 3. Results and discussions

### 268 3.1 NPF event frequency in Po Valley

269 During the measurement period, frequent NPF events occurred in Po Valley (Fig. 2, Fig. S1). On 27%  
270 of the days, we observed new particle formation with growth at the site, while on 39% of the days we

271 observed new particle formation without growth (Fig. S1). In total we observed new sub-3 nm clusters  
272 forming on 66 % of the days. Even though we applied the similar definition of NPF events as previous  
273 study, we can only compare our NPF events with growth type with the reported NPF event frequency  
274 due to the lack of capacity to measure the sub-3nm particles in previous literature. Our results were  
275 similar to those by Hamed et al. (2007) who observed NPF events on 36 % of the time in March and  
276 April of 2002 at the same site. Manninen et al. (2010) observed NPF events during more than half of  
277 all days from March to Oct in 2008 and Kontkanen et al. (2016) observed NPF during 89 % of the days  
278 in July at the same site, which is higher than our observations. Hamed et al. (2007) also observed that  
279 NPF with growth events on 60% of the days during summer, which suggests that summertime NPF  
280 frequency at SPC is typically higher than our observation in springtime 2022. This difference in the  
281 observed NPF frequency was likely due to the different season with favorable conditions for NPF such  
282 as potential lower CS (due to less stagnant meteorological conditions) and higher basic and organic  
283 molecule concentrations in summer. In addition, the abundant solar radiation and low aerosol water  
284 content (limiting surface area and heterogenous reactions (Du et al., 2022)), likely create favorable  
285 conditions for NPF to occur.

286 The median average particle formation rates at 1.7 nm, 3 nm and 7 nm for all sampling days with NPF  
287 with growth events were  $87 \text{ cm}^{-3} \text{ s}^{-1}$  ( $32 - 133 \text{ cm}^{-3} \text{ s}^{-1}$ ),  $3.2 \text{ cm}^{-3} \text{ s}^{-1}$  ( $1.4 \text{ cm}^{-3} \text{ s}^{-1} - 7.0 \text{ cm}^{-3} \text{ s}^{-1}$ ) and  $1.4$   
288  $\text{cm}^{-3} \text{ s}^{-1}$  ( $0.3 \text{ cm}^{-3} \text{ s}^{-1} - 3.0 \text{ cm}^{-3} \text{ s}^{-1}$ ), respectively. The formation rate at 1.7 nm during NPF with growth  
289 days (NPF with growth,  $87 \text{ cm}^{-3} \text{ s}^{-1}$ ) is similar to that observed previously at the same site by Kontkanen  
290 et al. (2016) in summer. The high formation rate, which is comparable with heavily polluted urban  
291 environments such as Beijing and Shanghai, China ( $59 \text{ cm}^{-3} \text{ s}^{-1} - 225 \text{ cm}^{-3} \text{ s}^{-1}$  (Deng et al., 2020; Yao  
292 et al., 2018)), will be further discussed in section 3.4. The average formation rate ( $J_{1.7}$ ) on NPF days  
293 without growth ( $24 \text{ cm}^{-3} \text{ s}^{-1}$ ) is much lower. During the noontime, the formation rate of particles for  
294 NPF events with no growth was less than half of  $J_{1.7}$  for NPF with growth (Fig. S2). It suggests that for  
295 particles to grow in a polluted environment such as the Po Valley, there needs to be abundant clustering  
296 to overcome losses to the existing condensation sink so that at least some of the particles survive to  
297 grow into larger sizes.

298 SA has long been known as a primary gaseous precursor for NPF in continental environments, owing  
299 to its extremely low volatility (Kirkby et al., 2011; Kulmala et al., 2013). During our sampling period,  
300 we observed high SA concentration in the Po Valley, in accordance with the frequent NPF events. The  
301 daily average SA concentration measured between 10:00 – 14:00 LT was  $4.6 \times 10^6 \text{ cm}^{-3}$ , which increased  
302 to  $8.5 \times 10^6 \text{ cm}^{-3}$  during NPF events with growth, aligning with previous findings from the same site  
303 ( $1.6 \times 10^7 \text{ cm}^{-3}$  during NPF in summer of 2009, (Paasonen et al., 2010)). Over the entire sampling period  
304 (10:00 – 14:00 LT), SA showed a moderately correlation with the calculated  $J_{1.7}$  ( $r = 0.49$ , Spearman  
305 correlation coefficient, for the logarithmic values), but its relationship varied among different days. This  
306 suggests that in addition to SA, other components, such as basic molecules, may also contribute to  
307 driving NPF events and subsequent growth in the Po Valley.

### 308 **3.2 Nucleation mechanism**

309 To investigate the NPF mechanism in the Po Valley, in this study we firstly compared the  
310 simultaneously measured  $J_{1.7}$  and SA with recent Cosmics Leaving Outdoor Droplets (CLOUD)  
311 chamber experiments that simulated NPF under polluted boundary layer conditions with anthropogenic  
312 emissions (Xiao et al., 2021). In those experiments, amines, ammonia, as well as aromatics were added  
313 to reflect a heavily anthropogenic emission-influenced environment. Certain basic molecules, including  
314 amines (e.g., dimethylamine (DMA)) and ammonia ( $\text{NH}_3$ ) have been shown to substantially enhance  
315 nucleation and reduce evaporation by stabilizing atmospheric SA in chamber studies (Almeida et al.,  
316 2013). Besides, OOMs can also contribute to NPF and subsequent particle growth, even without the  
317 inclusion of SA (Kirkby et al., 2016; Xiao et al., 2021). As shown in Fig. 3a, most of the measurements  
318 were above the SA- $\text{NH}_3$  system at 278K from the CLOUD chamber, suggesting the SA- $\text{NH}_3$  mechanism  
319 itself cannot solely explain the measured  $J_{1.7}$  and that other species are most likely participating to NPF

320 in the Po Valley. For instance, amines, such as DMA or TMA, with higher basicity may contribute to  
321 NPF, consistent with not negligible concentrations of amines in previous studies in the aerosol at SPC  
322 (Paglione et al., 2014; Decesari et al., 2014). For the whole sampling period, the median SA and  $J_{1.7}$   
323 values in Po Valley follows the SA-DMA-NH<sub>3</sub> (4 ppt DMA and 1ppb NH<sub>3</sub>) and SA-DMA-NH<sub>3</sub>-Org  
324 (adding additional oxidized aromatic organics (Xiao et al., 2021)) lines from the CLOUD chamber at  
325 293K even though during most of the NPF days the average noontime temperature was around 285K  
326 (Fig. 3a).

327 The SA dimer measured by CI-APi-TOF is typically used as an indicator for the initial step for the  
328 cluster formation in NPF events (Yan et al., 2021). According to a previous study (Yan et al., 2021),  
329 the source and sink terms of the SA dimer can be determined by calculating the formation rate from SA  
330 monomer collisions and the loss rate from the SA dimer through coagulation onto pre-existing particles  
331 (Fig. 2b). In general, the correlation coefficient between SA dimer and its source to sink term ratios ( $r$   
332 = 0.80, Spearman correlation coefficient) indicated that similar to Chinese urban areas, SA dimer was  
333 in a pseudo steady-state between the formation of SA monomer collision and the loss onto CS by  
334 coagulation.

335 To further assess the influence of DMA, one of the most common and efficient base molecules for NPF  
336 in urban environments (Yao et al., 2018), we compared the measured SA dimer concentrations with the  
337 simulated ones under different DMA levels (from 0.1 ppt to reaching kinetic limit) by the kinetic model  
338 (Fig. 3b). From our cluster kinetics simulations, during the peak hours of NPF, DMA concentrations  
339 are expected to be in the range of 0.1 ppt to 5 ppt, which is lower than the need for reaching the kinetic  
340 limit (Figs. 3b and S3). It implies that other factors, for example, the abundant ambient NH<sub>3</sub>  
341 concentrations (~10 ppb) or trimethylamine (TMA) during our study period may also participate in  
342 cluster formation. It is consistent with the Vocus measurement, which suggests the ambient DMA  
343 signals were close to the background levels (Fig. S4). The reason for not reaching SA-DMA limit during  
344 the campaign could be 1) the relatively lower DMA emissions (such as vehicle flows) than Chinese  
345 megacities (Ge et al., 2011; Zhu et al., 2022), and 2) the quickly scavenge caused by photolysis and  
346 nighttime high RH (85%) (Leng et al., 2015; Yao et al., 2016). Therefore, both of the abundant ambient  
347 NH<sub>3</sub> concentrations (~10 ppb) and amines likely participated in cluster formation during our study  
348 period.

349 Median particle growth rates (GR) during NPF events for 1.5 – 3 nm, 3 – 7 nm, 7 – 15 nm were 1.3  
350 (1.0– 2.4) nm h<sup>-1</sup>, 4.6 (2.9 – 5.8) nm h<sup>-1</sup>, and 5.1 (3.8 – 8.8) nm h<sup>-1</sup>, respectively. The values in brackets  
351 represent the 25<sup>th</sup> and the 75<sup>th</sup> percentile of data (Fig. 3c). Growth rates increase with particle diameters,  
352 a phenomenon observed in other campaigns around the world as well (Kontkanen et al., 2017, Kulmala  
353 et al., 2013)), typically indicative of an increasing organic vapors contribution with size (e.g.,  
354 Stolzenburg et al. (2018)). The growth rates observed here were similar to those observed by Kontkanen  
355 et al. (2016) at SPC in summer (7.2 nm h<sup>-1</sup> for 7 – 20 nm) and our 1.5 – 3 nm growth rate matches well  
356 with Manninen et al. (2010) (1.5 nm h<sup>-1</sup>) during spring in the Po Valley. A comparison to predicted  
357 growth rates from sulfuric acid condensation without organics, which was calculated based on kinetic  
358 collisions of the measured SA concentrations and the effect of van-der-Waals forces on the collision  
359 frequency ((Stolzenburg et al., 2020), Fig. 3c), suggests that sulfuric acid condensation may be on  
360 average sufficient for the growth of the smallest clusters. It supports the argument that in the initial  
361 steps of NPF and growth in Po Valley sulfuric acid and its stabilizing molecules (likely the bases NH<sub>3</sub>  
362 and amines) were controlling particle formation. However, for particles to grow beyond 3 nm in size  
363 other vapors were needed, which was suggested by the significantly lower contribution of growth by  
364 SA (indicated by the green line) than the measured GR for 3 – 7 nm and 7 – 15 nm (Fig. 3c). Those  
365 vapors were likely a mixture of organics of anthropogenic and biogenic origin (with the latter emitted  
366 at higher rates during summer, which could cause the slightly higher values in Kontkanen et al. (2017)).  
367 We compared the GR during NPF with and without growth events using the method proposed in  
368 Kulmala et al. (2022) where the signal was averaged for all classified non-event days and then an



369 appearance time fit was performed for each size channel independently, revealing also a growth pattern.  
370 We found no significant difference for the GR in 7 – 15 nm size range (GR=5.1 nm h<sup>-1</sup> in NPF with  
371 growth days and average GR=6.1 nm h<sup>-1</sup> in NPF without growth days). Considering the similar CS and  
372 GR levels for NPF with and without growth days, the higher formation rates at 1.7 nm (87 cm<sup>-3</sup> s<sup>-1</sup>) may  
373 be a more important factor to surpass the CS. In stable meteorological conditions, a higher formation  
374 rate may significantly elevate the possibility of newly formed particles overcome the CS and continuous  
375 grow to larger sizes.

### 376 **3.3 Ion and neutral clusters and further particle growth**

377 During the campaign, we observed and identified different types of ion clusters with cluster ion  
378 measurements using the APi-TOF, including SA-NH<sub>3</sub>, SA-Amine, SA-NH<sub>3</sub>-Amine, SA-NH<sub>3</sub>-Org  
379 during NPF. In Fig. 4a, we presented the mass defect plot of the naturally charged ion clusters on April  
380 20<sup>th</sup>, when strong NPF events were observed ( $J_{1.7}$ : 83 cm<sup>-3</sup> s<sup>-1</sup>). The presence of these clusters was  
381 usually in conjunction with SA tetramers (SA<sub>4</sub>), pentamers (SA<sub>5</sub>), and hexamers (SA<sub>6</sub>), which  
382 potentially contribute to the NPF events. In Api-TOF measurement, the absence of basic species in the  
383 smallest sulfuric acid clusters is likely attributed to the loss of base molecules within the mass  
384 spectrometer (Cai et al., 2022b; Zha et al., 2023; Alfaouri et al., 2022).

385 Among all SA-base (SA-B) clusters, the most abundant SA-NH<sub>3</sub> clusters were from SA<sub>4</sub>-B to SA<sub>6</sub>-B  
386 (Fig. 4a), even though they are reported to be more easily evaporated than DMA clusters due to  
387 collision-induced dissociation (Passananti et al., 2019). Pure SA-Amine clusters were only found in the  
388 SA<sub>4</sub>-B clusters with different types of amines, including methylamine (C<sub>1</sub>-amine), DMA (C<sub>2</sub>-amine),  
389 trimethylamine (C<sub>3</sub>-amine), and butylamine (C<sub>4</sub>-amine). The detection of other SA-B than SA-DMA  
390 clusters indicates that other candidate bases could also play a crucial role in the complex atmosphere  
391 for nucleation. For example, a recent study conducted in Beijing highlights the importance of TMA,  
392 which can enhance nucleation rate from SA-DMA system by 50% – 100% (Cai et al., 2023b). In the Po  
393 Valley, the signal intensity of SA<sub>4</sub>-NH<sub>3</sub> was significantly higher than that of the pure SA<sub>4</sub>-amine clusters  
394 (~2 times) even though amines (e.g., DMA) were proven to be more efficient (~3 orders of magnitude)  
395 than NH<sub>3</sub> in clustering (Almeida et al., 2013). SA-NH<sub>3</sub>-Amine clusters could be found along with SA-  
396 NH<sub>3</sub> clusters in SA<sub>5</sub>-B and SA<sub>6</sub>-B. Similar patterns of the high fractions of SA-NH<sub>3</sub> and SA-NH<sub>3</sub>-  
397 Amine clusters were also reported in the CLOUD chamber studies under relatively low DMA and high  
398 NH<sub>3</sub> conditions (Schobesberger et al., 2013). Therefore, it can be concluded that a large amount of NH<sub>3</sub>  
399 also participates in NPF in the Po Valley region. Meanwhile, with a much lower amount, amines may  
400 also play a crucial role in the formation of small clusters (SA-B) due to their high stabilization  
401 efficiencies.

402 Moreover, some SA-NH<sub>3</sub>-Org and I-containing ion clusters were also observed on NPF days, but to a  
403 much lower extent than clusters involving NH<sub>3</sub> or DMA. It has been shown in previous CLOUD  
404 chamber studies that the oxidation products of anthropogenic volatile organic compounds (AVOCs, e.g.,  
405 naphthalene, trimethylbenzene and toluene) can largely promote the formation rate of particles (Xiao  
406 et al., 2021). The I-containing ions (mainly IO<sub>3</sub><sup>-</sup>) likely originated from the Adriatic Sea during the  
407 daytime, which was indicated by the easterly wind. Since no large iodine clusters were identified in the  
408 APi-TOF (e.g., (HIO<sub>3</sub>)<sub>0-1</sub>(I<sub>2</sub>O<sub>5</sub>)<sub>n</sub>·IO<sub>3</sub><sup>-</sup>, (He et al., 2021)), iodine-induced new particle formation in the  
409 Po Valley may not be as important as the pristine marine environment (Sipila et al., 2016). During NPF  
410 without growth days, the formation mechanism was similar to the NPF days regarding the ion cluster  
411 measurement (Fig. S5).

412 The SA monomer in the Po Valley can be observed during the peak hours (10:00 – 14:00 LT) in both  
413 NPF and non-NPF days, but much lower SA dimer or trimers were found in the non-NPF days (Figs.  
414 4b, and S6). In the nighttime, the SA concentrations were close to zero due to the scavenging of SO<sub>2</sub>  
415 and SA by hydrated aerosol and hygroscopic growth of particles, as indicated by the high RH (Fig. 1).  
416 During our sampling period, large amounts of organics were identified by the CI-APi-TOF. They were

417 typically smaller than 400 Th with carbon numbers < 8 and oxygen numbers < 6 (Fig. S7). Due to the  
418 relatively high NO<sub>x</sub> levels (13 ppb) that can terminate the dimerization reactions (Yan et al., 2020), no  
419 OOM dimers were found, which is different from clean and biogenically dominated environments such  
420 as Hyytiälä (Lehtipalo et al., 2018). The compositions of OOMs were similar between NPF and non-  
421 NPF days but with different abundance. Extremely high abundances of nitrophenols and their  
422 homologous compounds were found on non-NPF days (~8 times higher than on NPF days), likely  
423 caused by both of the enhanced primary (e.g., biomass burning (Mohr et al., 2013) and pesticide usage  
424 (Harrison et al., 2005)) and secondary (e.g., photochemical and/or aqueous-phase secondary formation)  
425 sources (Zheng et al., 2021; Gilardoni et al., 2016). C<sub>2-4</sub>H<sub>4,5</sub>N<sub>0,1</sub>O<sub>3,4</sub> compounds were found to be 50%  
426 higher (Fig. S7) on non-NPF days due to the higher RH and the enhanced heterogeneous reactions that  
427 form smaller organics such as carboxylic acids. Previous studies also reported aqueous-phase organic  
428 aerosol processing at high RH (Gilardoni et al., 2016) and high concentrations of carboxylic acids such  
429 as formic, oxalic, and malonic acids in the springtime in the Po Valley (Saarikoski et al., 2012). In  
430 general, the fraction of the abundance of nitrogen-containing OOMs (CHON) of total identified OOMs  
431 were 60% – 70%, which is close to the levels reported in polluted cities such as Nanjing (Nie et al.,  
432 2022) and Beijing (Guo et al., 2022). A slightly higher fraction of CHON compounds (73 %) was found  
433 during non-NPF days than NPF days (67 %), consistent with higher NO<sub>x</sub> and fine particulate matter  
434 levels (Fig. S8). It is likely associated with the stagnant meteorological conditions and accumulation of  
435 pollutants during the non-NPF days. However, the overall high amounts of CHON compounds and the  
436 lack of organic dimers make it unlikely that OOMs drive the NPF process (both clustering and initial  
437 growth, see e.g., Simon et al. (2020)). Their similar abundance on non-NPF and NPF days was also in  
438 line with the similar estimated GR for both types of days.

439 Throughout the entire sampling period, relatively high concentrations of fine particulate matters (PM<sub>2.5</sub>)  
440 were measured, with a daily average of 17 μg m<sup>-3</sup> and a maximum value of 43 μg m<sup>-3</sup>. Correspondingly,  
441 the hourly CS levels, which quantify the ability of pre-existing particles to scavenge gaseous precursors,  
442 ranged from <1×10<sup>-4</sup> s<sup>-1</sup> to 3×10<sup>-2</sup> s<sup>-1</sup> with an average value of 5.4×10<sup>-3</sup> s<sup>-1</sup>. Previous studies in polluted  
443 areas, such as Chinese megacities, have shown that NPF events are closely linked to CS levels (Cai et  
444 al., 2017). NPF probability was reported to decreased to 50% when CS was around 1×10<sup>-2</sup> s<sup>-1</sup> and  
445 completely shut off with CS of 6×10<sup>-2</sup> s<sup>-1</sup> (Du et al., 2022). However, in the Po Valley, we observed no  
446 strong influence of CS on NPF events, with only a slightly difference in CS during the noontime of non-  
447 NPF days (median: 9.4×10<sup>-3</sup> s<sup>-1</sup>) than NPF days (median: 8.6×10<sup>-3</sup> s<sup>-1</sup>).

### 448 **3.4 Comparison between Po Valley and other environments**

449  
450 Even though the measured  $J_{1,7}$  in Po Valley was at the same level of the values found in Chinese polluted  
451 megacities, it was much higher than in clean environments, such as the boreal forest of Hyytiälä in  
452 Finland, mountain sites Jungfraujoch in Switzerland, and Chacaltaya in Bolivia (1.5 cm<sup>-3</sup> s<sup>-1</sup> – 2.0 cm<sup>-3</sup>  
453 s<sup>-1</sup>, Fig. 5a). The average SA concentrations (4.6×10<sup>6</sup> cm<sup>-3</sup>, 10:00 – 14:00 LT) were comparable to the  
454 levels observed in polluted megacities in China (ranging from 3.9×10<sup>6</sup> cm<sup>-3</sup> to 7.4×10<sup>6</sup> cm<sup>-3</sup>, Fig. 5c),  
455 but significantly higher than those in remote areas like Hyytiälä (9×10<sup>5</sup> cm<sup>-3</sup>) and the Jungfraujoch  
456 (5×10<sup>5</sup> cm<sup>-3</sup>). SA concentrations during NPF days (8.6×10<sup>6</sup> cm<sup>-3</sup>) in the Po Valley were twice as high  
457 as those on non-NPF days (4 ×10<sup>6</sup> cm<sup>-3</sup>). This difference may be linked to the significant variations (t-  
458 test, p<0.05) of SO<sub>2</sub> concentrations between NPF days (0.38 ppb) and non-NPF days (0.20 ppb). This  
459 contrasts with findings in Beijing, where similar or even higher levels of SA and SO<sub>2</sub> were observed  
460 during non-NPF days compared to NPF event days (Yan et al., 2021). The variations in SO<sub>2</sub> and SA  
461 concentrations in the Po Valley could possibly be attributed to differences of air masses, as indicated  
462 by higher RH on non-NPF days (53%) than on NPF days (38%) but similar temperature (NPF days:  
463 288 K, non-NPF days: 287 K). On higher RH days, photochemistry may be suppressed, potentially  
464 reducing the formation of sulfuric acid and low volatile condensable vapors.

465 The overall CS in spring (median:  $8.9 \times 10^{-3} \text{ s}^{-1}$ ) in the Po Valley was lower than that in other polluted  
466 cities ( $1.5 \times 10^{-1} \text{ s}^{-1}$ –  $2.0 \times 10^{-1} \text{ s}^{-1}$ ), but significantly higher than that in clean environments ( $2.0 \times 10^{-4} \text{ s}^{-1}$   
467 (Hyytiälä and Jungfraujoch) –  $3.0 \times 10^{-3} \text{ s}^{-1}$  (Chacaltaya with the influence of volcanoes), Fig. 5e).  
468 Contrary to Beijing or Shanghai where CS levels and efficiencies are the dominant factors for the NPF  
469 process (Du et al., 2022), NPF events in Po Valley are not strongly dependent on the CS levels ( $9.4 \times 10^{-3}$   
470  $\text{ s}^{-1}$  and  $8.6 \times 10^{-3} \text{ s}^{-1}$  for non-NPF and NPF days, respectively), likely due to generally lower CS levels  
471 than the Asian megacities (Fig. S8). The strength of precursor sources and their accumulation in the Po-  
472 Valley region might thus be more important for NPF to occur than the overall pre-existing sink for those  
473 precursors.

474 The average  $\text{PM}_{10}$  concentrations during the sampling period was around  $8 \mu\text{g m}^{-3}$ , significantly lower  
475 than New Delhi ( $268 \mu\text{g m}^{-3}$ ), Beijing ( $33 \mu\text{g m}^{-3}$ , (Li et al., 2019)) and Shanghai ( $30 \mu\text{g m}^{-3}$ , (Song et  
476 al., 2023), Fig. S9). The major chemical compositions in  $\text{PM}_{10}$  in Po Valley were similar to those in  
477 Beijing and Shanghai, with organics, ammonium nitrate, and ammonium sulfate being the most  
478 abundant components. However,  $\text{PM}_{10}$  compositions in New Delhi differed from Po Valley and  
479 megacities in China. In New Delhi, strong biomass burning emissions with a high abundance of primary  
480 organics ( $155 \mu\text{g m}^{-3}$ , 58%) suppressed NPF events during the daytime from January to February but  
481 led to nocturnal particle growth, which is not observed in other polluted areas (Mishra et al., 2023).

482 Even with similar levels of CS and total  $\text{PM}_{10}$  concentrations (NPF:  $6.3 \mu\text{g m}^{-3}$  and non-NPF:  $6.5 \mu\text{g m}^{-3}$   
483  $\text{ s}^{-1}$ ) observed during noontime in Po Valley, the concentration of  $\text{NO}_3^-$  increased by 50% on non-NPF  
484 days compared to NPF days, higher than the increase of  $\text{PM}_{10}$  (3.1%) as shown in Fig. S9. A lower CS  
485 efficiency on NPF days due to lower fraction of nitrate was reported to suppress the scavenge of NPF  
486 precursors in Beijing (Du et al., 2022), which may also have the similar influence in the Po Valley. The  
487 observed growth rate for 7 – 15 nm particles in the Po Valley was about  $5.1 \text{ nm h}^{-1}$ , comparable to other  
488 urban and remote sites ( $2.9$  –  $9.1 \text{ nm h}^{-1}$ , Fig. 5f). The general similar growth rates among different  
489 types of environments were also reported in previous studies (Deng et al., 2020), which needs further  
490 investigation in future research.

491 For the basic gaseous precursors, the average concentration of  $\text{NH}_3$  was  $\sim 10$  ppb, which was in the same  
492 range as that found in the Chinese megacities (10 – 30 ppb) and much higher than that at remote sites  
493 ( $< 0.1$  ppb, Table S1). The high  $\text{NH}_3$  can be attributed to agricultural activities such as fertilization,  
494 which were widely applied during springtime in the region. The strong interference of ammonia emitted  
495 from fertilization to NPF was also observed in Quidja, an agricultural site in Southern Finland (Olin et  
496 al., 2022). During our sampling period, measured DMA were too close to the detection limit of the  
497 Vocus (Fig. S2), and lower than those observed in the Chinese megacities (10 – 40 ppt, Fig. 5d). In the  
498 spring season, DMA in the Po Valley cannot fully stabilize all atmospheric SA clusters and hence NPF  
499 is very sensitive to variations in the concentrations of the different stabilizers ( $\text{NH}_3$ , DMA, and as shown  
500 by our analysis likely only to a lower extent organics). This could explain the scattered correlation  
501 between the formation rate and SA concentrations on different days (Fig. 3).

502 Therefore, in the Po Valley region, the initial nucleation of frequent NPF is primarily attributed to high  
503 sulfuric acid concentrations and basic molecules, including ammonia and various amines. This  
504 mechanism is generally similar to what is observed in Chinese megacities. However, in the Po Valley  
505 region, DMA, a typical base in anthropogenic emission-influenced areas, is insufficient to stabilize the  
506 high levels of sulfuric acid, leading to the involvement of other basic molecules like additional other  
507 type of amines and ammonia, likely originating from fertilization in the area. This involvement of  
508 ammonia and other amines differs from Chinese megacities such as Shanghai, where high levels of  
509 DMA were observed ( $\sim 40$  ppt, (Yao et al., 2018; Yao et al., 2016)). As insufficient DMA is available  
510 to stabilize all clusters, we speculate that the clustering is therefore sensitive to the abundance of amines  
511 and the variations in DMA or other amine concentrations would result in different formation rates. In  
512 that sense, during our sampling period, NPF in Po Valley seems to be more sensitive to the strength of  
513 certain emission sources of amines compared to megacity environments, where the clustering is  
514 “saturated” with respect to DMA (i.e., proceeding at the maximum kinetically possible rate). The

515 abundant OOMs dominate the consecutive growth process, leading to a comparable GR to Chinese  
516 megacities such as Beijing and Shanghai. Due to the relatively lower CS than these megacities, the  
517 newly formed particles may however have a higher survival probability compared to the megacities and  
518 provide more long-term surviving particles in the Po Valley, indicating a decisive role of NPF for Po-  
519 Valley aerosol and PM<sub>2.5</sub> concentrations.

#### 520 **4. Conclusions**

521 In this study, we conducted a continuous two-month measurement campaign in the Italian Po Valley  
522 during springtime, where frequent NPF events were observed on 66% of all days. Through direct ion  
523 cluster measurement, kinetic models, and the comparison with the CLOUD chamber experiment, we  
524 have determined that sulfuric acid-base nucleation is the dominant formation mechanism in the Po  
525 Valley region. Abundant sulfuric acid and basic molecules, including amines and ammonia derived  
526 from agriculture activities, provided ample precursors for NPF events. In contrast to megacity  
527 environments, CS showed no significant difference between NPF event and non-event days, indicating  
528 that in Po Valley it is more the abundance of precursors than the variations in the sink controlling the  
529 occurrence of NPF. Furthermore, we observed that apart from DMA, a typical basic precursor, NH<sub>3</sub> and  
530 other amines were also likely to be involved in NPF in the Po Valley. This was supported by the high  
531 abundance of SA-NH<sub>3</sub> and SA-amine-NH<sub>3</sub> clusters measured by the APi-TOF during NPF events. DMA,  
532 while more efficient than ammonia, was insufficient to stabilize all SA during our sampling period.  
533 This resulted in a more scattered correlation between sulfuric acid concentrations and measured  
534 formation rates compared to Chinese megacities. In that sense, we could show that the clustering during  
535 NPF is clearly distinct between polluted megacity environments and polluted semi-urbanized regions  
536 such as Po Valley. Similar to Beijing, we found that OOMs did not play a decisive role in the initial  
537 cluster formations, likely due to the absence of ultra-low volatility organics (typical OOM dimers) in  
538 the ions and neutral cluster measurements. However, low-volatility organics were abundant enough to  
539 induce fast growth processes above 3 nm. The comparable GR and formation rates, along with lower  
540 efficient CS compared to megacity environments, indicate a high survival probability for the newly  
541 formed particles. Therefore, NPF is likely to play an important role in the fine particle concentrations  
542 and pollution levels in the Po Valley region. Further reductions of key NPF species, including SO<sub>2</sub>,  
543 amines and NH<sub>3</sub>, can contribute to suppressing NPF event frequency and lowering particle numbers.  
544 This, in turn, would improve air quality in the Po Valley region.

#### 545 **Data availability**

546 Data are available from the authors upon request.

#### 547 **Competing interests**

548 At least one of the (co-)authors is a member of the editorial board of Atmospheric Chemistry and  
549 Physics

#### 550 **Author contributions**

551 JC, DS, FB, and MK designed the research. JC, JS, YFG, SH, MP, AN, FM, SD, MR, NZ and CM  
552 collected the data at the SPC site. JC, JS, YG, ST, RY, DA, QZ, DS and FB interpreted the data. MP,  
553 WH, YL, GC, LQ, KL, YG, CW, WN, JK, CM, QZ, DS, FB helped to improve the manuscript. JC, JS,  
554 DS, and FB wrote the manuscript with contributions from all co-authors. All authors have given  
555 approval to the final version of this manuscript.

#### 556 **Acknowledgements**

557 The work is supported by the Academy of Finland (Center of Excellence in Atmospheric Sciences,  
558 project no. 307331, PROF13 funding no. 311932, and ACCC Flagship no. 337549), the European  
559 Research Council via ATM-GTP (no. 742206), Consolidator grant INTEGRATE (no. 865799) and

560 CHAPAs (no. 850614), the European Union’s Horizon 2020 research and innovation programme  
561 (project FORCeS under grant agreement no. 821205, H2020-INFRAIA-2020-1 grant agreement no.  
562 101008004, Marie Skłodowska–Curie grant agreement no. 895875 (NPF-PANDA), the Vienna Science  
563 and Technology Fund (WWTF) through project VRG22-003, Jenny and Antti Wihuri Foundation, and  
564 the Knut and Alice Wallenberg Foundation (WAF project CLOUDFORM, grant no. 2017.0165). The  
565 authors also would like to thank the effort from all the researchers in the SPC site. The authors would  
566 also like to thank Chenjuan Deng, Mao Xiao and Lubna Dada for providing the supporting data in  
567 Beijing and CLOUD chamber experiment.

568

569 **Reference**

- 570 Almeida, J., Schobesberger, S., Kurten, A., Ortega, I. K., Kupiainen-Maatta, O., Praplan, A. P., Adamov,  
571 A., Amorim, A., Bianchi, F., Breitenlechner, M., David, A., Dommen, J., Donahue, N. M., Downard, A.,  
572 Dunne, E., Duplissy, J., Ehrhart, S., Flagan, R. C., Franchin, A., Guida, R., Hakala, J., Hansel, A.,  
573 Heinritzi, M., Henschel, H., Jokinen, T., Junninen, H., Kajos, M., Kangasluoma, J., Keskinen, H., Kupc,  
574 A., Kurten, T., Kvashin, A. N., Laaksonen, A., Lehtipalo, K., Leiminger, M., Leppa, J., Loukonen, V.,  
575 Makhmutov, V., Mathot, S., McGrath, M. J., Nieminen, T., Olenius, T., Onnela, A., Petaja, T.,  
576 Riccobono, F., Riipinen, I., Rissanen, M., Rondo, L., Ruuskanen, T., Santos, F. D., Sarnela, N.,  
577 Schallhart, S., Schnitzhofer, R., Seinfeld, J. H., Simon, M., Sipila, M., Stozhkov, Y., Stratmann, F.,  
578 Tome, A., Trostl, J., Tsagkogeorgas, G., Vaattovaara, P., Viisanen, Y., Virtanen, A., Vrtala, A., Wagner,  
579 P. E., Weingartner, E., Wex, H., Williamson, C., Wimmer, D., Ye, P., Yli-Juuti, T., Carslaw, K. S.,  
580 Kulmala, M., Curtius, J., Baltensperger, U., Worsnop, D. R., Vehkamäki, H., and Kirkby, J.: Molecular  
581 understanding of sulphuric acid-amine particle nucleation in the atmosphere, *Nature*, 502, 359-363,  
582 10.1038/nature12663, 2013.
- 583 Boulon, J., Sellegri, K., Venzac, H., Picard, D., Weingartner, E., Wehrle, G., Collaud Coen, M.,  
584 Bütikofer, R., Flückiger, E., Baltensperger, U., and Laj, P.: New particle formation and ultrafine  
585 charged aerosol climatology at a high altitude site in the Alps (Jungfraujoch, 3580 m a.s.l.,  
586 Switzerland), *Atmospheric Chemistry and Physics*, 10, 9333-9349, 10.5194/acp-10-9333-2010, 2010.
- 587 Brean, J., Beddows, D. C. S., Shi, Z., Temime-Roussel, B., Marchand, N., Querol, X., Alastuey, A.,  
588 Minguillón, M. C., and Harrison, R. M.: Molecular insights into new particle formation in Barcelona,  
589 Spain, *Atmospheric Chemistry and Physics*, 20, 10029-10045, 10.5194/acp-20-10029-2020, 2020.
- 590 Cai, J., Daellenbach, K. R., Wu, C., Zheng, Y., Zheng, F., Du, W., Haslett, S. L., Chen, Q., Kulmala, M.,  
591 and Mohr, C.: Characterization of offline analysis of particulate matter with FIGAERO-CIMS,  
592 *Atmospheric Measurement Techniques*, 16, 1147-1165, 10.5194/amt-16-1147-2023, 2023a.
- 593 Cai, J., Wu, C., Wang, J., Du, W., Zheng, F., Hakala, S., Fan, X., Chu, B., Yao, L., Feng, Z., Liu, Y., Sun, Y.,  
594 Zheng, J., Yan, C., Bianchi, F., Kulmala, M., Mohr, C., and Daellenbach, K. R.: Influence of organic  
595 aerosol molecular composition on particle absorptive properties in autumn Beijing, *Atmospheric*  
596 *Chemistry and Physics*, 22, 1251-1269, 10.5194/acp-22-1251-2022, 2022.
- 597 Cai, R., Attoui, M., Jiang, J., Korhonen, F., Hao, J., Petäjä, T., and Kangasluoma, J.: Characterization of  
598 a high-resolution supercritical differential mobility analyzer at reduced flow rates, *Aerosol Science*  
599 *and Technology*, 52, 1332-1343, 10.1080/02786826.2018.1520964, 2018.
- 600 Cai, R., Yang, D., Fu, Y., Wang, X., Li, X., Ma, Y., Hao, J., Zheng, J., and Jiang, J.: Aerosol surface area  
601 concentration: a governing factor in new particle formation in Beijing, *Atmospheric Chemistry and*  
602 *Physics*, 17, 12327-12340, 10.5194/acp-17-12327-2017, 2017.
- 603 Cai, R., Yin, R., Li, X., Xie, H.-B., Yang, D., Kerminen, V.-M., Smith, J. N., Ma, Y., Hao, J., Chen, J.,  
604 Kulmala, M., Zheng, J., Jiang, J., and Elm, J.: Significant contributions of trimethylamine to sulfuric  
605 acid nucleation in polluted environments, *npj Climate and Atmospheric Science*, 6, 10.1038/s41612-  
606 023-00405-3, 2023b.
- 607 Cai, R., Yan, C., Yang, D., Yin, R., Lu, Y., Deng, C., Fu, Y., Ruan, J., Li, X., Kontkanen, J., Zhang, Q.,  
608 Kangasluoma, J., Ma, Y., Hao, J., Worsnop, D. R., Bianchi, F., Paasonen, P., Kerminen, V. M., Liu, Y.,  
609 Wang, L., Zheng, J., Kulmala, M., and Jiang, J.: Sulfuric acid-amine nucleation in urban Beijing,  
610 *Atmos. Chem. Phys.*, 21, 2457-2468, 10.5194/acp-21-2457-2021, 2021.
- 611 Chu, B., Kerminen, V.-M., Bianchi, F., Yan, C., Petäjä, T., and Kulmala, M.: Atmospheric new particle  
612 formation in China, *Atmospheric Chemistry and Physics*, 19, 115-138, 10.5194/acp-19-115-2019,  
613 2019.
- 614 Dada, L., Chellapermal, R., Buenrostro Mazon, S., Paasonen, P., Lampilahti, J., Manninen, H. E.,  
615 Junninen, H., Petäjä, T., Kerminen, V.-M., and Kulmala, M.: Refined classification and  
616 characterization of atmospheric new-particle formation events using air ions, *Atmospheric*  
617 *Chemistry and Physics*, 18, 17883-17893, 10.5194/acp-18-17883-2018, 2018.
- 618 Dai, L., Wang, H., Zhou, L., An, J., Tang, L., Lu, C., Yan, W., Liu, R., Kong, S., Chen, M., Lee, S., and Yu,  
619 H.: Regional and local new particle formation events observed in the Yangtze River Delta region,

620 China, *Journal of Geophysical Research: Atmospheres*, 122, 2389-2402, 10.1002/2016jd026030,  
621 2017.

622 Dal Maso, M., Kulmala, M., Riipinen, I., Wagner, R., Hussein, T., Aalto, P. P., and Lehtinen, K. E. J.:  
623 Formation and growth of fresh atmospheric aerosols: eight years of aerosol size distribution data  
624 from SMEAR II, Hyytiälä, Finland, *Boreal Environment Research*, 10, 323-336, 2005.

625 de Jesus, A. L., Rahman, M. M., Mazaheri, M., Thompson, H., Knibbs, L. D., Jeong, C., Evans, G., Nei,  
626 W., Ding, A., Qiao, L., Li, L., Portin, H., Niemi, J. V., Timonen, H., Luoma, K., Petaja, T., Kulmala, M.,  
627 Kowalski, M., Peters, A., Cyrus, J., Ferrero, L., Manigrasso, M., Avino, P., Buonano, G., Reche, C.,  
628 Querol, X., Beddows, D., Harrison, R. M., Sowlat, M. H., Sioutas, C., and Morawska, L.: Ultrafine  
629 particles and PM<sub>2.5</sub> in the air of cities around the world: Are they representative of each other?,  
630 *Environ Int*, 129, 118-135, 10.1016/j.envint.2019.05.021, 2019.

631 Decesari, S., Allan, J., Plass-Duelmer, C., Williams, B. J., Paglione, M., Facchini, M. C., O'Dowd, C.,  
632 Harrison, R. M., Gietl, J. K., Coe, H., Giulianelli, L., Gobbi, G. P., Lanconelli, C., Carbone, C., Worsnop,  
633 D., Lambe, A. T., Ahern, A. T., Moretti, F., Tagliavini, E., Elste, T., Gilge, S., Zhang, Y., and Dall'Osto,  
634 M.: Measurements of the aerosol chemical composition and mixing state in the Po Valley using  
635 multiple spectroscopic techniques, *Atmospheric Chemistry and Physics*, 14, 12109-12132,  
636 10.5194/acp-14-12109-2014, 2014.

637 Deng, C., Fu, Y., Dada, L., Yan, C., Cai, R., Yang, D., Zhou, Y., Yin, R., Lu, Y., Li, X., Qiao, X., Fan, X., Nie,  
638 W., Kontkanen, J., Kangasluoma, J., Chu, B., Ding, A., Kerminen, V. M., Paasonen, P., Worsnop, D. R.,  
639 Bianchi, F., Liu, Y., Zheng, J., Wang, L., Kulmala, M., and Jiang, J.: Seasonal Characteristics of New  
640 Particle Formation and Growth in Urban Beijing, *Environ Sci Technol*, 54, 8547-8557,  
641 10.1021/acs.est.0c00808, 2020.

642 Du, W., Cai, J., Zheng, F., Yan, C., Zhou, Y., Guo, Y., Chu, B., Yao, L., Heikkinen, L. M., Fan, X., Wang, Y.,  
643 Cai, R., Hakala, S., Chan, T., Kontkanen, J., Tuovinen, S., Petäjä, T., Kangasluoma, J., Bianchi, F.,  
644 Paasonen, P., Sun, Y., Kerminen, V.-M., Liu, Y., Daellenbach, K. R., Dada, L., and Kulmala, M.:  
645 Influence of Aerosol Chemical Composition on Condensation Sink Efficiency and New Particle  
646 Formation in Beijing, *Environmental Science & Technology Letters*, 9, 375-382,  
647 10.1021/acs.estlett.2c00159, 2022.

648 Fan, X., Cai, J., Yan, C., Zhao, J., Guo, Y., Li, C., Dällenbach, K. R., Zheng, F., Lin, Z., Chu, B., Wang, Y.,  
649 Dada, L., Zha, Q., Du, W., Kontkanen, J., Kurtén, T., Iyer, S., Kujansuu, J. T., Petäjä, T., Worsnop, D. R.,  
650 Kerminen, V.-M., Liu, Y., Bianchi, F., Tham, Y. J., Yao, L., and Kulmala, M.: Atmospheric gaseous  
651 hydrochloric and hydrobromic acid in urban Beijing, China: detection, source identification and  
652 potential atmospheric impacts, *Atmospheric Chemistry and Physics*, 21, 11437-11452, 10.5194/acp-  
653 21-11437-2021, 2021.

654 Fernández de la Mora, J. and Kozlowski, J.: Hand-held differential mobility analyzers of high  
655 resolution for 1–30nm particles: Design and fabrication considerations, *Journal of Aerosol Science*,  
656 57, 45-53, 10.1016/j.jaerosci.2012.10.009, 2013.

657 Fu, Y., Xue, M., Cai, R., Kangasluoma, J., and Jiang, J.: Theoretical and experimental analysis of the  
658 core sampling method: Reducing diffusional losses in aerosol sampling line, *Aerosol Science and  
659 Technology*, 53, 793-801, 10.1080/02786826.2019.1608354, 2019.

660 Gilardoni, S., Massoli, P., Paglione, M., Giulianelli, L., Carbone, C., Rinaldi, M., Decesari, S., Sandrini,  
661 S., Costabile, F., Gobbi, G. P., Pietrogrande, M. C., Visentin, M., Scotto, F., Fuzzi, S., and Facchini, M.  
662 C.: Direct observation of aqueous secondary organic aerosol from biomass-burning emissions, *Proc  
663 Natl Acad Sci U S A*, 113, 10013-10018, 10.1073/pnas.1602212113, 2016.

664 Guo, S., Hu, M., Zamora, M. L., Peng, J., Shang, D., Zheng, J., Du, Z., Wu, Z., Shao, M., Zeng, L.,  
665 Molina, M. J., and Zhang, R.: Elucidating severe urban haze formation in China, *Proc Natl Acad Sci U S  
666 A*, 111, 17373-17378, 10.1073/pnas.1419604111, 2014.

667 Guo, S., Hu, M., Peng, J., Wu, Z., Zamora, M. L., Shang, D., Du, Z., Zheng, J., Fang, X., Tang, R., Wu, Y.,  
668 Zeng, L., Shuai, S., Zhang, W., Wang, Y., Ji, Y., Li, Y., Zhang, A. L., Wang, W., Zhang, F., Zhao, J., Gong,  
669 X., Wang, C., Molina, M. J., and Zhang, R.: Remarkable nucleation and growth of ultrafine particles

670 from vehicular exhaust, *Proceedings of the National Academy of Sciences*,  
671 10.1073/pnas.1916366117, 2020.

672 Guo, Y., Yan, C., Liu, Y., Qiao, X., Zheng, F., Zhang, Y., Zhou, Y., Li, C., Fan, X., Lin, Z., Feng, Z., Zhang,  
673 Y., Zheng, P., Tian, L., Nie, W., Wang, Z., Huang, D., Daellenbach, K. R., Yao, L., Dada, L., Bianchi, F.,  
674 Jiang, J., Liu, Y., Kerminen, V.-M., and Kulmala, M.: Seasonal variation in oxygenated organic  
675 molecules in urban Beijing and their contribution to secondary organic aerosol, *Atmospheric  
676 Chemistry and Physics*, 22, 10077-10097, 10.5194/acp-22-10077-2022, 2022.

677 Hamed, A., Joutsensaari, J., Mikkonen, S., Sogacheva, L., Dal Maso, M., Kulmala, M., Cavalli, F., Fuzzi,  
678 S., Facchini, M. C., Decesari, S., Mircea, M., Lehtinen, K. E. J., and Laaksonen, A.: Nucleation and  
679 growth of new particles in Po Valley, Italy, *Atmos. Chem. Phys.*, 7, 355-376, 10.5194/acp-7-355-2007,  
680 2007.

681 Harrison, M. A. J., Barra, S., Borghesi, D., Vione, D., Arsene, C., and Iulian Olariu, R.: Nitrated phenols  
682 in the atmosphere: a review, *Atmospheric Environment*, 39, 231-248,  
683 10.1016/j.atmosenv.2004.09.044, 2005.

684 He, X. C., Tham, Y. J., Dada, L., Wang, M., Finkenzeller, H., Stolzenburg, D., Iyer, S., Simon, M., Kurten,  
685 A., Shen, J., Rorup, B., Rissanen, M., Schobesberger, S., Baalbaki, R., Wang, D. S., Koenig, T. K.,  
686 Jokinen, T., Sarnela, N., Beck, L. J., Almeida, J., Amanatidis, S., Amorim, A., Ataei, F., Baccarini, A.,  
687 Bertozzi, B., Bianchi, F., Brilke, S., Caudillo, L., Chen, D., Chiu, R., Chu, B., Dias, A., Ding, A., Dommen,  
688 J., Duplissy, J., El Haddad, I., Gonzalez Carracedo, L., Granzin, M., Hansel, A., Heinritzi, M., Hofbauer,  
689 V., Junninen, H., Kangasluoma, J., Kempainen, D., Kim, C., Kong, W., Krechmer, J. E., Kvashin, A.,  
690 Laitinen, T., Lamkaddam, H., Lee, C. P., Lehtipalo, K., Leiminger, M., Li, Z., Makhmutov, V., Manninen,  
691 H. E., Marie, G., Marten, R., Mathot, S., Mauldin, R. L., Mentler, B., Mohler, O., Muller, T., Nie, W.,  
692 Onnela, A., Petaja, T., Pfeifer, J., Philippov, M., Ranjithkumar, A., Saiz-Lopez, A., Salma, I., Scholz, W.,  
693 Schuchmann, S., Schulze, B., Steiner, G., Stozhkov, Y., Tauber, C., Tome, A., Thakur, R. C., Vaisanen,  
694 O., Vazquez-Pufleau, M., Wagner, A. C., Wang, Y., Weber, S. K., Winkler, P. M., Wu, Y., Xiao, M., Yan,  
695 C., Ye, Q., Ylisirnio, A., Zauner-Wieczorek, M., Zha, Q., Zhou, P., Flagan, R. C., Curtius, J.,  
696 Baltensperger, U., Kulmala, M., Kerminen, V. M., Kurten, T., Donahue, N. M., Volkamer, R., Kirkby, J.,  
697 Worsnop, D. R., and Sipila, M.: Role of iodine oxoacids in atmospheric aerosol nucleation, *Science*,  
698 371, 589-595, 10.1126/science.abe0298, 2021.

699 Jokinen, T., Sipilä, M., Junninen, H., Ehn, M., Lönn, G., Hakala, J., Petäjä, T., Mauldin, R. L., Kulmala,  
700 M., and Worsnop, D. R.: Atmospheric sulphuric acid and neutral cluster measurements using CI-API-  
701 TOF, *Atmospheric Chemistry and Physics*, 12, 4117-4125, 10.5194/acp-12-4117-2012, 2012.

702 Junninen, H., Ehn, M., Petäjä, T., Luosujärvi, L., Kotiaho, T., Kostianen, R., Rohner, U., Gonin, M.,  
703 Fuhrer, K., Kulmala, M., and Worsnop, D. R.: A high-resolution mass spectrometer to measure  
704 atmospheric ion composition, *Atmospheric Measurement Techniques*, 3, 1039-1053, 10.5194/amt-  
705 3-1039-2010, 2010.

706 Kangasluoma, J., Ahonen, L. R., Laurila, T. M., Cai, R., Enroth, J., Mazon, S. B., Korhonen, F., Aalto, P.  
707 P., Kulmala, M., Attoui, M., and Petäjä, T.: Laboratory verification of a new high flow differential  
708 mobility particle sizer, and field measurements in Hyytiälä, *Journal of Aerosol Science*, 124, 1-9,  
709 10.1016/j.jaerosci.2018.06.009, 2018.

710 Kangasluoma, J., Attoui, M., Junninen, H., Lehtipalo, K., Samodurov, A., Korhonen, F., Sarnela, N.,  
711 Schmidt-Ott, A., Worsnop, D., Kulmala, M., and Petäjä, T.: Sizing of neutral sub 3nm tungsten oxide  
712 clusters using Airmodus Particle Size Magnifier, *Journal of Aerosol Science*, 87, 53-62,  
713 10.1016/j.jaerosci.2015.05.007, 2015.

714 Kangasluoma, J., Franchin, A., Duplissy, J., Ahonen, L., Korhonen, F., Attoui, M., Mikkilä, J., Lehtipalo,  
715 K., Vanhanen, J., Kulmala, M., and Petäjä, T.: Operation of the Airmodus A11 nano Condensation  
716 Nucleus Counter at various  
717 inlet pressures and various operation temperatures, and design of a new inlet  
718 system, *Atmospheric Measurement Techniques*, 9, 2977-2988, 10.5194/amt-9-2977-2016, 2016.



719 Kirkby, J., Curtius, J., Almeida, J., Dunne, E., Duplissy, J., Ehrhart, S., Franchin, A., Gagne, S., Ickes, L.,  
720 Kurten, A., Kupc, A., Metzger, A., Riccobono, F., Rondo, L., Schobesberger, S., Tsagkogeorgas, G.,  
721 Wimmer, D., Amorim, A., Bianchi, F., Breitenlechner, M., David, A., Dommen, J., Downard, A., Ehn,  
722 M., Flagan, R. C., Haider, S., Hansel, A., Hauser, D., Jud, W., Junninen, H., Kreissl, F., Kvashin, A.,  
723 Laaksonen, A., Lehtipalo, K., Lima, J., Lovejoy, E. R., Makhmutov, V., Mathot, S., Mikkilä, J.,  
724 Minginette, P., Mogo, S., Nieminen, T., Onnela, A., Pereira, P., Petaja, T., Schnitzhofer, R., Seinfeld, J.  
725 H., Sipila, M., Stozhkov, Y., Stratmann, F., Tome, A., Vanhanen, J., Viisanen, Y., Vrtala, A., Wagner, P.  
726 E., Walther, H., Weingartner, E., Wex, H., Winkler, P. M., Carslaw, K. S., Worsnop, D. R.,  
727 Baltensperger, U., and Kulmala, M.: Role of sulphuric acid, ammonia and galactic cosmic rays in  
728 atmospheric aerosol nucleation, *Nature*, 476, 429-433, 10.1038/nature10343, 2011.

729 Kirkby, J., Duplissy, J., Sengupta, K., Frege, C., Gordon, H., Williamson, C., Heinritzi, M., Simon, M.,  
730 Yan, C., Almeida, J., Trostl, J., Nieminen, T., Ortega, I. K., Wagner, R., Adamov, A., Amorim, A.,  
731 Bernhammer, A. K., Bianchi, F., Breitenlechner, M., Brilke, S., Chen, X., Craven, J., Dias, A., Ehrhart, S.,  
732 Flagan, R. C., Franchin, A., Fuchs, C., Guida, R., Hakala, J., Hoyle, C. R., Jokinen, T., Junninen, H.,  
733 Kangasluoma, J., Kim, J., Krapf, M., Kurten, A., Laaksonen, A., Lehtipalo, K., Makhmutov, V., Mathot,  
734 S., Molteni, U., Onnela, A., Perakyla, O., Piel, F., Petaja, T., Praplan, A. P., Pringle, K., Rap, A.,  
735 Richards, N. A., Riipinen, I., Rissanen, M. P., Rondo, L., Sarnela, N., Schobesberger, S., Scott, C. E.,  
736 Seinfeld, J. H., Sipila, M., Steiner, G., Stozhkov, Y., Stratmann, F., Tome, A., Virtanen, A., Vogel, A. L.,  
737 Wagner, A. C., Wagner, P. E., Weingartner, E., Wimmer, D., Winkler, P. M., Ye, P., Zhang, X., Hansel,  
738 A., Dommen, J., Donahue, N. M., Worsnop, D. R., Baltensperger, U., Kulmala, M., Carslaw, K. S., and  
739 Curtius, J.: Ion-induced nucleation of pure biogenic particles, *Nature*, 533, 521-526,  
740 10.1038/nature17953, 2016.

741 Kontkanen, J., Järvinen, E., Manninen, H. E., Lehtipalo, K., Kangasluoma, J., Decesari, S., Gobbi, G. P.,  
742 Laaksonen, A., Petäjä, T., and Kulmala, M.: High concentrations of sub-3nm clusters and frequent  
743 new particle formation observed in the Po Valley, Italy, during the PEGASOS 2012 campaign,  
744 *Atmospheric Chemistry and Physics*, 16, 1919-1935, 10.5194/acp-16-1919-2016, 2016.

745 Kontkanen, J., Lehtipalo, K., Ahonen, L., Kangasluoma, J., Manninen, H. E., Hakala, J., Rose, C.,  
746 Sellegri, K., Xiao, S., Wang, L., Qi, X., Nie, W., Ding, A., Yu, H., Lee, S., Kerminen, V.-M., Petäjä, T., and  
747 Kulmala, M.: Measurements of sub-3 nm particles using a particle size magnifier in different  
748 environments: from clean mountain top to polluted megacities, *Atmospheric Chemistry and Physics*,  
749 17, 2163-2187, 10.5194/acp-17-2163-2017, 2017.

750 Kulmala, M., Kerminen, V. M., Petäjä, T., Ding, A. J., and Wang, L.: Atmospheric gas-to-particle  
751 conversion: why NPF events are observed in megacities?, *Faraday Discussions*, 200, 271-288,  
752 10.1039/C6FD00257A, 2017.

753 Kulmala, M., Petäjä, T., Nieminen, T., Sipilä, M., Manninen, H. E., Lehtipalo, K., Dal Maso, M., Aalto,  
754 P. P., Junninen, H., Paasonen, P., Riipinen, I., Lehtinen, K. E. J., Laaksonen, A., and Kerminen, V.-M.:  
755 Measurement of the nucleation of atmospheric aerosol particles, *Nature Protocols*, 7, 1651-1667,  
756 10.1038/nprot.2012.091, 2012.

757 Kulmala, M., Junninen, H., Dada, L., Salma, I., Weidinger, T., Thén, W., Vörösmarty, M., Komsaare, K.,  
758 Stolzenburg, D., Cai, R., Yan, C., Li, X., Deng, C., Jiang, J., Petäjä, T., Nieminen, T., and Kerminen, V.-  
759 M.: Quiet New Particle Formation in the Atmosphere, *Frontiers in Environmental Science*, 10,  
760 10.3389/fenvs.2022.912385, 2022.

761 Kulmala, M., Kontkanen, J., Junninen, H., Lehtipalo, K., Manninen, H. E., Nieminen, T., Petäjä, T.,  
762 Sipilä, M., Schobesberger, S., Rantala, P., Franchin, A., Jokinen, T., Järvinen, E., Äijälä, M.,  
763 Kangasluoma, J., Hakala, J., Aalto, P. P., Paasonen, P., Mikkilä, J., Vanhanen, J., Aalto, J., Hakola, H.,  
764 Makkonen, U., Ruuskanen, T., Mauldin, R. L., Duplissy, J., Vehkamäki, H., Bäck, J., Kortelainen, A.,  
765 Riipinen, I., Kurtén, T., Johnston, M. V., Smith, J. N., Ehn, M., Mentel, T. F., Lehtinen, K. E. J.,  
766 Laaksonen, A., Kerminen, V.-M., and Worsnop, D. R.: Direct Observations of Atmospheric Aerosol  
767 Nucleation, *Science*, 339, 943-946, 10.1126/science.1227385, 2013.

768 Kulmala, M., Dada, L., Daellenbach, K. R., Yan, C., Stolzenburg, D., Kontkanen, J., Ezhova, E., Hakala,  
769 S., Tuovinen, S., Kokkonen, T. V., Kurppa, M., Cai, R., Zhou, Y., Yin, R., Baalbaki, R., Chan, T., Chu, B.,

770 Deng, C., Fu, Y., Ge, M., He, H., Heikkinen, L., Junninen, H., Liu, Y., Lu, Y., Nie, W., Rusanen, A.,  
771 Vakkari, V., Wang, Y., Yang, G., Yao, L., Zheng, J., Kujansuu, J., Kangasluoma, J., Petaja, T., Paasonen,  
772 P., Jarvi, L., Worsnop, D., Ding, A., Liu, Y., Wang, L., Jiang, J., Bianchi, F., and Kerminen, V. M.: Is  
773 reducing new particle formation a plausible solution to mitigate particulate air pollution in Beijing  
774 and other Chinese megacities?, *Faraday Discuss*, 226, 334-347, 10.1039/d0fd00078g, 2021.

775 Kurten, A., Rondo, L., Ehrhart, S., and Curtius, J.: Calibration of a chemical ionization mass  
776 spectrometer for the measurement of gaseous sulfuric acid, *J Phys Chem A*, 116, 6375-6386,  
777 10.1021/jp212123n, 2012.

778 Lampimäki, M., Baalbaki, R., Ahonen, L., Korhonen, F., Cai, R., Chan, T., Stolzenburg, D., Petäjä, T.,  
779 Kangasluoma, J., Vanhanen, J., and Lehtipalo, K.: Novel aerosol diluter – Size dependent  
780 characterization down to 1 nm particle size, *Journal of Aerosol Science*, 172, 106180,  
781 <https://doi.org/10.1016/j.jaerosci.2023.106180>, 2023.

782 Lehtipalo, K., Ahonen, L. R., Baalbaki, R., Sulo, J., Chan, T., Laurila, T., Dada, L., Duplissy, J., Miettinen,  
783 E., Vanhanen, J., Kangasluoma, J., Kulmala, M., Petäjä, T., and Jokinen, T.: The standard operating  
784 procedure for Airmodus Particle Size Magnifier and nano-Condensation Nucleus Counter, *Journal of*  
785 *Aerosol Science*, 159, 10.1016/j.jaerosci.2021.105896, 2022.

786 Lehtipalo, K., Yan, C., Dada, L., Bianchi, F., Xiao, M., Wagner, R., Stolzenburg, D., Ahonen, L. R.,  
787 Amorim, A., Baccharini, A., Bauer, P. S., Baumgartner, B., Bergen, A., Bernhammer, A.-K.,  
788 Breitenlechner, M., Brilke, S., Buchholz, A., Mazon, S. B., Chen, D., Chen, X., Dias, A., Dommen, J.,  
789 Draper, D. C., Duplissy, J., Ehn, M., Finkenzeller, H., Fischer, L., Frege, C., Fuchs, C., Garmash, O.,  
790 Gordon, H., Hakala, J., He, X., Heikkinen, L., Heinritzi, M., Helm, J. C., Hofbauer, V., Hoyle, C. R.,  
791 Jokinen, T., Kangasluoma, J., Kerminen, V.-M., Kim, C., Kirkby, J., Kontkanen, J., Kürten, A., Lawler, M.  
792 J., Mai, H., Mathot, S., Mauldin, R. L., Molteni, U., Nichman, L., Nie, W., Nieminen, T., Ojdanic, A.,  
793 Onnela, A., Passananti, M., Petäjä, T., Piel, F., Pospisilova, V., Quéléver, L. L. J., Rissanen, M. P., Rose,  
794 C., Sarnela, N., Schallhart, S., Schuchmann, S., Sengupta, K., Simon, M., Sipilä, M., Tauber, C., Tomé,  
795 A., Tröstl, J., Väisänen, O., Vogel, A. L., Volkamer, R., Wagner, A. C., Wang, M., Weitz, L., Wimmer, D.,  
796 Ye, P., Ylisirniö, A., Zha, Q., Carslaw, K. S., Curtius, J., Donahue, N. M., Flagan, R. C., Hansel, A.,  
797 Riipinen, I., Virtanen, A., Winkler, P. M., Baltensperger, U., Kulmala, M., and Worsnop, D. R.:  
798 Multicomponent new particle formation from sulfuric acid, ammonia, and biogenic vapors, *Science*  
799 *Advances*, 4, eaau5363, doi:10.1126/sciadv.aau5363, 2018.

800 Li, H., Cheng, J., Zhang, Q., Zheng, B., Zhang, Y., Zheng, G., and He, K.: Rapid transition in winter  
801 aerosol composition in Beijing from 2014 to 2017: response to clean air actions, *Atmospheric*  
802 *Chemistry and Physics*, 19, 11485-11499, 10.5194/acp-19-11485-2019, 2019.

803 Liu, S., Hu, M., Wu, Z., Wehner, B., Wiedensohler, A., and Cheng, Y.: Aerosol number size distribution  
804 and new particle formation at a rural/coastal site in Pearl River Delta (PRD) of China, *Atmospheric*  
805 *Environment*, 42, 6275-6283, 10.1016/j.atmosenv.2008.01.063, 2008.

806 Manninen, H. E., Nieminen, T., Asmi, E., Gagné, S., Häkkinen, S., Lehtipalo, K., Aalto, P., Vana, M.,  
807 Mirme, A., Mirme, S., Hörrak, U., Plass-Dülmer, C., Stange, G., Kiss, G., Hoffer, A., Törő, N., Moerman,  
808 M., Henzing, B., de Leeuw, G., Brinkenberg, M., Kouvarakis, G. N., Bougiatioti, A., Mihalopoulos, N.,  
809 O'Dowd, C., Ceburnis, D., Arneth, A., Svenningsson, B., Swietlicki, E., Tarozzi, L., Decesari, S., Facchini,  
810 M. C., Birmili, W., Sonntag, A., Wiedensohler, A., Boulon, J., Sellegri, K., Laj, P., Gysel, M., Bukowiecki,  
811 N., Weingartner, E., Wehrle, G., Laaksonen, A., Hamed, A., Joutsensaari, J., Petäjä, T., Kerminen, V.  
812 M., and Kulmala, M.: EUCAARI ion spectrometer measurements at 12 European sites – analysis of  
813 new particle formation events, *Atmos. Chem. Phys.*, 10, 7907-7927, 10.5194/acp-10-7907-2010,  
814 2010.

815 Mishra, S., Tripathi, S. N., Kanawade, V. P., Haslett, S. L., Dada, L., Ciarelli, G., Kumar, V., Singh, A.,  
816 Bhattu, D., Rastogi, N., Daellenbach, K. R., Ganguly, D., Gargava, P., Slowik, J. G., Kulmala, M., Mohr,  
817 C., El-Haddad, I., and Prevot, A. S. H.: Rapid night-time nanoparticle growth in Delhi driven by  
818 biomass-burning emissions, *Nature Geoscience*, 16, 224-230, 10.1038/s41561-023-01138-x, 2023.

819 Mohr, C., Lopez-Hilfiker, F. D., Zotter, P., Prevot, A. S., Xu, L., Ng, N. L., Herndon, S. C., Williams, L. R.,  
820 Franklin, J. P., Zahniser, M. S., Worsnop, D. R., Knighton, W. B., Aiken, A. C., Gorkowski, K. J., Dubey,

821 M. K., Allan, J. D., and Thornton, J. A.: Contribution of nitrated phenols to wood burning brown  
822 carbon light absorption in Detling, United Kingdom during winter time, *Environ Sci Technol*, 47,  
823 6316-6324, 10.1021/es400683v, 2013.

824 Nie, W., Yan, C., Huang, D. D., Wang, Z., Liu, Y., Qiao, X., Guo, Y., Tian, L., Zheng, P., Xu, Z., Li, Y., Xu,  
825 Z., Qi, X., Sun, P., Wang, J., Zheng, F., Li, X., Yin, R., Dallenbach, K. R., Bianchi, F., Petäjä, T., Zhang, Y.,  
826 Wang, M., Schervish, M., Wang, S., Qiao, L., Wang, Q., Zhou, M., Wang, H., Yu, C., Yao, D., Guo, H.,  
827 Ye, P., Lee, S., Li, Y. J., Liu, Y., Chi, X., Kerminen, V.-M., Ehn, M., Donahue, N. M., Wang, T., Huang, C.,  
828 Kulmala, M., Worsnop, D., Jiang, J., and Ding, A.: Secondary organic aerosol formed by condensing  
829 anthropogenic vapours over China's megacities, *Nature Geoscience*, 15, 255-261, 10.1038/s41561-  
830 022-00922-5, 2022.

831 Paasonen, P., Nieminen, T., Asmi, E., Manninen, H. E., Petäjä, T., Plass-Dülmer, C., Flentje, H., Birmili,  
832 W., Wiedensohler, A., Hörrak, U., Metzger, A., Hamed, A., Laaksonen, A., Facchini, M. C., Kerminen,  
833 V. M., and Kulmala, M.: On the roles of sulphuric acid and low-volatility organic vapours in the initial  
834 steps of atmospheric new particle formation, *Atmospheric Chemistry and Physics*, 10, 11223-11242,  
835 10.5194/acp-10-11223-2010, 2010.

836 Paglione, M., Decesari, S., Rinaldi, M., Tarozzi, L., Manarini, F., Gilardoni, S., Facchini, M. C., Fuzzi, S.,  
837 Bacco, D., Trentini, A., Pandis, S. N., and Nenes, A.: Historical Changes in Seasonal Aerosol Acidity in  
838 the Po Valley (Italy) as Inferred from Fog Water and Aerosol Measurements, *Environ Sci Technol*, 55,  
839 7307-7315, 10.1021/acs.est.1c00651, 2021.

840 Paglione, M., Saarikoski, S., Carbone, S., Hillamo, R., Facchini, M. C., Finessi, E., Giulianelli, L.,  
841 Carbone, C., Fuzzi, S., Moretti, F., Tagliavini, E., Swietlicki, E., Eriksson Stenström, K., Prévôt, A. S. H.,  
842 Massoli, P., Canaragatna, M., Worsnop, D., and Decesari, S.: Primary and secondary biomass burning  
843 aerosols determined by proton nuclear magnetic resonance ( $^1\text{H-NMR}$ )  
844 spectroscopy during the 2008 EUCAARI campaign in the Po Valley (Italy), *Atmospheric Chemistry and  
845 Physics*, 14, 5089-5110, 10.5194/acp-14-5089-2014, 2014.

846 Paglione, M., Gilardoni, S., Rinaldi, M., Decesari, S., Zanca, N., Sandrini, S., Giulianelli, L., Bacco, D.,  
847 Ferrari, S., Poluzzi, V., Scotto, F., Trentini, A., Poulain, L., Herrmann, H., Wiedensohler, A., Canonaco,  
848 F., Prévôt, A. S. H., Massoli, P., Carbone, C., Facchini, M. C., and Fuzzi, S.: The impact of biomass  
849 burning and aqueous-phase processing on air quality: a multi-year source apportionment study in  
850 the Po Valley, Italy, *Atmospheric Chemistry and Physics*, 20, 1233-1254, 10.5194/acp-20-1233-2020,  
851 2020.

852 Passananti, M., Zapadinsky, E., Zanca, T., Kangasluoma, J., Myllys, N., Rissanen, M. P., Kurten, T., Ehn,  
853 M., Attoui, M., and Vehkamäki, H.: How well can we predict cluster fragmentation inside a mass  
854 spectrometer?, *Chem Commun (Camb)*, 55, 5946-5949, 10.1039/c9cc02896j, 2019.

855 Peineke, C., Attoui, M. B., and Schmidt-Ott, A.: Using a glowing wire generator for production of  
856 charged, uniformly sized nanoparticles at high concentrations, *Journal of Aerosol Science*, 37, 1651-  
857 1661, 10.1016/j.jaerosci.2006.06.006, 2006.

858 Peng, J. F., Hu, M., Wang, Z. B., Huang, X. F., Kumar, P., Wu, Z. J., Guo, S., Yue, D. L., Shang, D. J.,  
859 Zheng, Z., and He, L. Y.: Submicron aerosols at thirteen diversified sites in China: size distribution,  
860 new particle formation and corresponding contribution to cloud condensation nuclei production,  
861 *Atmos. Chem. Phys.*, 14, 10249-10265, 10.5194/acp-14-10249-2014, 2014.

862 Rose, C., Sellegri, K., Velarde, F., Moreno, I., Ramonet, M., Weinhold, K., Krejci, R., Ginot, P.,  
863 Andrade, M., Wiedensohler, A., and Laj, P.: Frequent nucleation events at the high altitude station of  
864 Chacaltaya (5240 m a.s.l.), Bolivia, *Atmospheric Environment*, 102, 18-29,  
865 10.1016/j.atmosenv.2014.11.015, 2015.

866 Saarikoski, S., Carbone, S., Decesari, S., Giulianelli, L., Angelini, F., Canaragatna, M., Ng, N. L.,  
867 Trimborn, A., Facchini, M. C., Fuzzi, S., Hillamo, R., and Worsnop, D.: Chemical characterization of  
868 springtime submicrometer aerosol in Po Valley, Italy, *Atmospheric Chemistry and Physics*, 12, 8401-  
869 8421, 10.5194/acp-12-8401-2012, 2012.

870 Schobesberger, S., Junninen, H., Bianchi, F., Lonn, G., Ehn, M., Lehtipalo, K., Dommen, J., Ehrhart, S.,  
871 Ortega, I. K., Franchin, A., Nieminen, T., Riccobono, F., Hutterli, M., Duplissy, J., Almeida, J., Amorim,

872 A., Breitenlechner, M., Downard, A. J., Dunne, E. M., Flagan, R. C., Kajos, M., Keskinen, H., Kirkby, J.,  
873 Kupc, A., Kurten, A., Kurten, T., Laaksonen, A., Mathot, S., Onnela, A., Praplan, A. P., Rondo, L.,  
874 Santos, F. D., Schallhart, S., Schnitzhofer, R., Sipila, M., Tome, A., Tsagkogeorgas, G., Vehkamäki, H.,  
875 Wimmer, D., Baltensperger, U., Carslaw, K. S., Curtius, J., Hansel, A., Petaja, T., Kulmala, M.,  
876 Donahue, N. M., and Worsnop, D. R.: Molecular understanding of atmospheric particle formation  
877 from sulfuric acid and large oxidized organic molecules, *Proc Natl Acad Sci U S A*, 110, 17223-17228,  
878 10.1073/pnas.1306973110, 2013.

879 Schraufnagel, D. E.: The health effects of ultrafine particles, *Exp Mol Med*, 52, 311-317,  
880 10.1038/s12276-020-0403-3, 2020.

881 Sebastian, M., Kompalli, S. K., Kumar, V. A., Jose, S., Babu, S. S., Pandithurai, G., Singh, S., Hooda, R.  
882 K., Soni, V. K., Pierce, J. R., Vakkari, V., Asmi, E., Westervelt, D. M., Hyvärinen, A.-P., and Kanawade,  
883 V. P.: Observations of particle number size distributions and new particle formation in six Indian  
884 locations, *Atmospheric Chemistry and Physics*, 22, 4491-4508, 10.5194/acp-22-4491-2022, 2022.

885 Shen, J., Bigi, A., Marinoni, A., Lampilahti, J., Kontkanen, J., Ciarelli, G., Putaud, J. P., Nieminen, T.,  
886 Kulmala, M., Lehtipalo, K., and Bianchi, F.: Emerging Investigator Series: COVID-19 lockdown effects  
887 on aerosol particle size distributions in northern Italy, *Environ Sci Atmos*, 1, 214-227,  
888 10.1039/d1ea00016k, 2021.

889 Shen, X. J., Sun, J. Y., Zhang, Y. M., Wehner, B., Nowak, A., Tuch, T., Zhang, X. C., Wang, T. T., Zhou, H.  
890 G., Zhang, X. L., Dong, F., Birmili, W., and Wiedensohler, A.: First long-term study of particle number  
891 size distributions and new particle formation events of regional aerosol in the North China Plain,  
892 *Atmospheric Chemistry and Physics*, 11, 1565-1580, 10.5194/acp-11-1565-2011, 2011.

893 Simon, M., Dada, L., Heinritzi, M., Scholz, W., Stolzenburg, D., Fischer, L., Wagner, A. C., Kürten, A.,  
894 Rörup, B., He, X.-C., Almeida, J., Baalbaki, R., Baccharini, A., Bauer, P. S., Beck, L., Bergen, A., Bianchi,  
895 F., Bräkling, S., Brilke, S., Caudillo, L., Chen, D., Chu, B., Dias, A., Draper, D. C., Duplissy, J., El-Haddad,  
896 I., Finkenzeller, H., Frege, C., Gonzalez-Carracedo, L., Gordon, H., Granzin, M., Hakala, J., Hofbauer,  
897 V., Hoyle, C. R., Kim, C., Kong, W., Lamkaddam, H., Lee, C. P., Lehtipalo, K., Leiminger, M., Mai, H.,  
898 Manninen, H. E., Marie, G., Marten, R., Mentler, B., Molteni, U., Niehman, L., Nie, W., Ojdanic, A.,  
899 Onnela, A., Partoll, E., Petäjä, T., Pfeifer, J., Philippov, M., Quéléver, L. L. J., Ranjithkumar, A.,  
900 Rissanen, M. P., Schallhart, S., Schobesberger, S., Schuchmann, S., Shen, J., Sipilä, M., Steiner, G.,  
901 Stozhkov, Y., Tauber, C., Tham, Y. J., Tomé, A. R., Vazquez-Pufleau, M., Vogel, A. L., Wagner, R.,  
902 Wang, M., Wang, D. S., Wang, Y., Weber, S. K., Wu, Y., Xiao, M., Yan, C., Ye, P., Ye, Q., Zauner-  
903 Wieczorek, M., Zhou, X., Baltensperger, U., Dommen, J., Flagan, R. C., Hansel, A., Kulmala, M.,  
904 Volkamer, R., Winkler, P. M., Worsnop, D. R., Donahue, N. M., Kirkby, J., and Curtius, J.: Molecular  
905 understanding of new-particle formation from  $\alpha$ -pinene between  $-50$  and  $+25$  °C,  
906 *Atmospheric Chemistry and Physics*, 20, 9183-9207, 10.5194/acp-20-9183-2020, 2020.

907 Sipila, M., Sarnela, N., Jokinen, T., Henschel, H., Junninen, H., Kontkanen, J., Richters, S.,  
908 Kangasluoma, J., Franchin, A., Perakyla, O., Rissanen, M. P., Ehn, M., Vehkamäki, H., Kurten, T.,  
909 Berndt, T., Petaja, T., Worsnop, D., Ceburnis, D., Kerminen, V. M., Kulmala, M., and O'Dowd, C.:  
910 Molecular-scale evidence of aerosol particle formation via sequential addition of HIO<sub>3</sub>, *Nature*, 537,  
911 532-534, 10.1038/nature19314, 2016.

912 Song, Z., Gao, W., Shen, H., Jin, Y., Zhang, C., Luo, H., Pan, L., Yao, B., Zhang, Y., Huo, J., Sun, Y., Yu,  
913 D., Chen, H., Chen, J., Duan, Y., Zhao, D., and Xu, J.: Roles of Regional Transport and Vertical Mixing  
914 in Aerosol Pollution in Shanghai Over the COVID-19 Lockdown Period Observed Above Urban  
915 Canopy, *Journal of Geophysical Research: Atmospheres*, 128, e2023JD038540,  
916 <https://doi.org/10.1029/2023JD038540>, 2023.

917 Stolzenburg, D., Fischer, L., Vogel, A. L., Heinritzi, M., Schervish, M., Simon, M., Wagner, A. C., Dada,  
918 L., Ahonen, L. R., Amorim, A., Baccharini, A., Bauer, P. S., Baumgartner, B., Bergen, A., Bianchi, F.,  
919 Breitenlechner, M., Brilke, S., Buenrostro Mazon, S., Chen, D., Dias, A., Draper, D. C., Duplissy, J., El  
920 Haddad, I., Finkenzeller, H., Frege, C., Fuchs, C., Garmash, O., Gordon, H., He, X., Helm, J., Hofbauer,  
921 V., Hoyle, C. R., Kim, C., Kirkby, J., Kontkanen, J., Kurten, A., Lampilahti, J., Lawler, M., Lehtipalo, K.,  
922 Leiminger, M., Mai, H., Mathot, S., Mentler, B., Molteni, U., Nie, W., Nieminen, T., Nowak, J. B.,

923 Ojdanic, A., Onnela, A., Passananti, M., Petaja, T., Quelever, L. L. J., Rissanen, M. P., Sarnela, N.,  
924 Schallhart, S., Tauber, C., Tome, A., Wagner, R., Wang, M., Weitz, L., Wimmer, D., Xiao, M., Yan, C.,  
925 Ye, P., Zha, Q., Baltensperger, U., Curtius, J., Dommen, J., Flagan, R. C., Kulmala, M., Smith, J. N.,  
926 Worsnop, D. R., Hansel, A., Donahue, N. M., and Winkler, P. M.: Rapid growth of organic aerosol  
927 nanoparticles over a wide tropospheric temperature range, *Proc Natl Acad Sci U S A*, 115, 9122-  
928 9127, 10.1073/pnas.1807604115, 2018.

929 Stolzenburg, D., Simon, M., Ranjithkumar, A., Kürten, A., Lehtipalo, K., Gordon, H., Ehrhart, S.,  
930 Finkenzeller, H., Pichelstorfer, L., Nieminen, T., He, X.-C., Brilke, S., Xiao, M., Amorim, A., Baalbaki, R.,  
931 Baccarini, A., Beck, L., Bräkling, S., Caudillo Murillo, L., Chen, D., Chu, B., Dada, L., Dias, A., Dommen,  
932 J., Duplissy, J., El Haddad, I., Fischer, L., Gonzalez Carracedo, L., Heinritzi, M., Kim, C., Koenig, T. K.,  
933 Kong, W., Lamkaddam, H., Lee, C. P., Leiminger, M., Li, Z., Makhmutov, V., Manninen, H. E., Marie,  
934 G., Marten, R., Müller, T., Nie, W., Partoll, E., Petäjä, T., Pfeifer, J., Philippov, M., Rissanen, M. P.,  
935 Rörup, B., Schobesberger, S., Schuchmann, S., Shen, J., Sipilä, M., Steiner, G., Stozhkov, Y., Tauber, C.,  
936 Tham, Y. J., Tomé, A., Vazquez-Pufleau, M., Wagner, A. C., Wang, M., Wang, Y., Weber, S. K.,  
937 Wimmer, D., Wlasits, P. J., Wu, Y., Ye, Q., Zauner-Wieczorek, M., Baltensperger, U., Carslaw, K. S.,  
938 Curtius, J., Donahue, N. M., Flagan, R. C., Hansel, A., Kulmala, M., Lelieveld, J., Volkamer, R., Kirkby,  
939 J., and Winkler, P. M.: Enhanced growth rate of atmospheric particles from sulfuric acid,  
940 *Atmospheric Chemistry and Physics*, 20, 7359-7372, 10.5194/acp-20-7359-2020, 2020.

941 Ude, S. and de la Mora, J. F.: Molecular monodisperse mobility and mass standards from  
942 electrosprays of tetra-alkyl ammonium halides, *Journal of Aerosol Science*, 36, 1224-1237,  
943 <https://doi.org/10.1016/j.jaerosci.2005.02.009>, 2005.

944 Vana, M., Komsaare, K., Hörrak, U., Mirme, S., Nieminen, T., Kontkanen, J., Manninen, H. E., Petäjä,  
945 T., Noe, S. M., and Kulmala, M.: Characteristics of new-particle formation at three SMEAR stations,  
946 *Boreal Environment Research*, 2016.

947 Vanhanen, J., Mikkilä, J., Lehtipalo, K., Sipilä, M., Manninen, H. E., Siivola, E., Petäjä, T., and Kulmala,  
948 M.: Particle Size Magnifier for Nano-CN Detection, *Aerosol Science and Technology*, 45, 533-542,  
949 10.1080/02786826.2010.547889, 2011.

950 Wang, Z., Wu, Z., Yue, D., Shang, D., Guo, S., Sun, J., Ding, A., Wang, L., Jiang, J., Guo, H., Gao, J.,  
951 Cheung, H. C., Morawska, L., Keywood, M., and Hu, M.: New particle formation in China: Current  
952 knowledge and further directions, *Science of The Total Environment*, 577, 258-266,  
953 10.1016/j.scitotenv.2016.10.177, 2017.

954 Wang, Z. B., Hu, M., Pei, X. Y., Zhang, R. Y., Paasonen, P., Zheng, J., Yue, D. L., Wu, Z. J., Boy, M., and  
955 Wiedensohler, A.: Connection of organics to atmospheric new particle formation and growth at an  
956 urban site of Beijing, *Atmospheric Environment*, 103, 7-17, 10.1016/j.atmosenv.2014.11.069, 2015.

957 Wang, Z. B., Hu, M., Sun, J. Y., Wu, Z. J., Yue, D. L., Shen, X. J., Zhang, Y. M., Pei, X. Y., Cheng, Y. F.,  
958 and Wiedensohler, A.: Characteristics of regional new particle formation in urban and regional  
959 background environments in the North China Plain, *Atmospheric Chemistry and Physics*, 13, 12495-  
960 12506, 10.5194/acp-13-12495-2013, 2013.

961 Wu, Z., Hu, M., Yue, D., Wehner, B., and Wiedensohler, A.: Evolution of particle number size  
962 distribution in an urban atmosphere during episodes of heavy pollution and new particle formation,  
963 *Science China Earth Sciences*, 54, 1772-1778, 10.1007/s11430-011-4227-9, 2011.

964 Wu, Z., Hu, M., Liu, S., Wehner, B., Bauer, S., Maßling, A., Wiedensohler, A., Petäjä, T., Dal Maso, M.,  
965 and Kulmala, M.: New particle formation in Beijing, China: Statistical analysis of a 1-year data set,  
966 *Journal of Geophysical Research*, 112, 10.1029/2006jd007406, 2007.

967 Xiao, M., Hoyle, C. R., Dada, L., Stolzenburg, D., Kürten, A., Wang, M., Lamkaddam, H., Garmash, O.,  
968 Mentler, B., Molteni, U., Baccarini, A., Simon, M., He, X.-C., Lehtipalo, K., Ahonen, L. R., Baalbaki, R.,  
969 Bauer, P. S., Beck, L., Bell, D., Bianchi, F., Brilke, S., Chen, D., Chiu, R., Dias, A., Duplissy, J.,  
970 Finkenzeller, H., Gordon, H., Hofbauer, V., Kim, C., Koenig, T. K., Lampilahti, J., Lee, C. P., Li, Z., Mai,  
971 H., Makhmutov, V., Manninen, H. E., Marten, R., Mathot, S., Mauldin, R. L., Nie, W., Onnela, A.,  
972 Partoll, E., Petäjä, T., Pfeifer, J., Pospisilova, V., Quéléver, L. L. J., Rissanen, M., Schobesberger, S.,  
973 Schuchmann, S., Stozhkov, Y., Tauber, C., Tham, Y. J., Tomé, A., Vazquez-Pufleau, M., Wagner, A. C.,

974 Wagner, R., Wang, Y., Weitz, L., Wimmer, D., Wu, Y., Yan, C., Ye, P., Ye, Q., Zha, Q., Zhou, X., Amorim,  
975 A., Carslaw, K., Curtius, J., Hansel, A., Volkamer, R., Winkler, P. M., Flagan, R. C., Kulmala, M.,  
976 Worsnop, D. R., Kirkby, J., Donahue, N. M., Baltensperger, U., El Haddad, I., and Dommen, J.: The  
977 driving factors of new particle formation and growth in the polluted boundary layer, *Atmospheric*  
978 *Chemistry and Physics*, 21, 14275-14291, 10.5194/acp-21-14275-2021, 2021.

979 Xiao, S., Wang, M. Y., Yao, L., Kulmala, M., Zhou, B., Yang, X., Chen, J. M., Wang, D. F., Fu, Q. Y.,  
980 Worsnop, D. R., and Wang, L.: Strong atmospheric new particle formation in winter in urban  
981 Shanghai, China, *Atmospheric Chemistry and Physics*, 15, 1769-1781, 10.5194/acp-15-1769-2015,  
982 2015.

983 Yan, C., Yin, R., Lu, Y., Dada, L., Yang, D., Fu, Y., Kontkanen, J., Deng, C., Garmash, O., Ruan, J.,  
984 Baalbaki, R., Schervish, M., Cai, R., Bloss, M., Chan, T., Chen, T., Chen, Q., Chen, X., Chen, Y., Chu, B.,  
985 Dällenbach, K., Foreback, B., He, X., Heikkinen, L., Jokinen, T., Junninen, H., Kangasluoma, J.,  
986 Kokkonen, T., Kurppa, M., Lehtipalo, K., Li, H., Li, H., Li, X., Liu, Y., Ma, Q., Paasonen, P., Rantala, P.,  
987 Pileci, R. E., Rusanen, A., Sarnela, N., Simonen, P., Wang, S., Wang, W., Wang, Y., Xue, M., Yang, G.,  
988 Yao, L., Zhou, Y., Kujansuu, J., Petäjä, T., Nie, W., Ma, Y., Ge, M., He, H., Donahue, N. M., Worsnop, D.  
989 R., Veli-Matti, K., Wang, L., Liu, Y., Zheng, J., Kulmala, M., Jiang, J., and Bianchi, F.: The Synergistic  
990 Role of Sulfuric Acid, Bases, and Oxidized Organics Governing New-Particle Formation in Beijing,  
991 *Geophysical Research Letters*, 48, 10.1029/2020gl091944, 2021.

992 Yan, C., Nie, W., Vogel, A. L., Dada, L., Lehtipalo, K., Stolzenburg, D., Wagner, R., Rissanen, M. P.,  
993 Xiao, M., Ahonen, L., Fischer, L., Rose, C., Bianchi, F., Gordon, H., Simon, M., Heinritzi, M., Garmash,  
994 O., Roldin, P., Dias, A., Ye, P., Hofbauer, V., Amorim, A., Bauer, P. S., Bergen, A., Bernhammer, A.-K.,  
995 Breitenlechner, M., Brilke, S., Buchholz, A., Mazon, S. B., Canagaratna, M. R., Chen, X., Ding, A.,  
996 Dommen, J., Draper, D. C., Duplissy, J., Frege, C., Heyn, C., Guida, R., Hakala, J., Heikkinen, L., Hoyle,  
997 C. R., Jokinen, T., Kangasluoma, J., Kirkby, J., Kontkanen, J., Kürten, A., Lawler, M. J., Mai, H., Mathot,  
998 S., Mauldin, R. L., Molteni, U., Nichman, L., Nieminen, T., Nowak, J., Ojdanic, A., Onnela, A., Pajunoja,  
999 A., Petäjä, T., Piel, F., Quéléver, L. L. J., Sarnela, N., Schallhart, S., Sengupta, K., Sipilä, M., Tomé, A.,  
1000 Tröstl, J., Väisänen, O., Wagner, A. C., Ylisirniö, A., Zha, Q., Baltensperger, U., Carslaw, K. S., Curtius,  
1001 J., Flagan, R. C., Hansel, A., Riipinen, I., Smith, J. N., Virtanen, A., Winkler, P. M., Donahue, N. M.,  
1002 Kerminen, V.-M., Kulmala, M., Ehn, M., and Worsnop, D. R.: Size-dependent influence of  
1003 NO<sub>x</sub> on the growth rates of organic aerosol particles, *Science Advances*, 6, eaay4945,  
1004 doi:10.1126/sciadv.aay4945, 2020.

1005 Yao, L., Wang, M.-Y., Wang, X.-K., Liu, Y.-J., Chen, H.-F., Zheng, J., Nie, W., Ding, A.-J., Geng, F.-H.,  
1006 Wang, D.-F., Chen, J.-M., Worsnop, D. R., and Wang, L.: Detection of atmospheric gaseous amines  
1007 and amides by a high-resolution time-of-flight chemical ionization mass spectrometer with  
1008 protonated ethanol reagent ions, *Atmospheric Chemistry and Physics*, 16, 14527-14543,  
1009 10.5194/acp-16-14527-2016, 2016.

1010 Yao, L., Garmash, O., Bianchi, F., Zheng, J., Yan, C., Kontkanen, J., Junninen, H., Mazon, S. B., Ehn, M.,  
1011 Paasonen, P., Sipilä, M., Wang, M. Y., Wang, X. K., Xiao, S., Chen, H. F., Lu, Y. Q., Zhang, B. W., Wang,  
1012 D. F., Fu, Q. Y., Geng, F. H., Li, L., Wang, H. L., Qiao, L. P., Yang, X., Chen, J. M., Kerminen, V. M.,  
1013 Petaja, T., Worsnop, D. R., Kulmala, M., and Wang, L.: Atmospheric new particle formation from  
1014 sulfuric acid and amines in a Chinese megacity, *Science*, 361, 278+, 10.1126/science.aao4839, 2018.

1015 Yu, H., Zhou, L., Dai, L., Shen, W., Dai, W., Zheng, J., Ma, Y., and Chen, M.: Nucleation and growth of  
1016 sub-3 nm particles in the polluted urban atmosphere of a megacity in China, *Atmospheric Chemistry*  
1017 *and Physics*, 16, 2641-2657, 10.5194/acp-16-2641-2016, 2016.

1018 Yue, D. L., Hu, M., Wang, Z. B., Wen, M. T., Guo, S., Zhong, L. J., Wiedensohler, A., and Zhang, Y. H.:  
1019 Comparison of particle number size distributions and new particle formation between the urban and  
1020 rural sites in the PRD region, China, *Atmospheric Environment*, 76, 181-188,  
1021 10.1016/j.atmosenv.2012.11.018, 2013.

1022 Zha, Q., Huang, W., Aliaga, D., Peräkylä, O., Heikkinen, L., Koenig, A. M., Wu, C., Enroth, J., Gramlich,  
1023 Y., Cai, J., Carbone, S., Hansel, A., Petäjä, T., Kulmala, M., Worsnop, D., Sinclair, V., Krejci, R.,  
1024 Andrade, M., Mohr, C., and Bianchi, F.: Measurement report: Molecular-level investigation of

1025 atmospheric cluster ions at the tropical high-altitude research station Chacaltaya (5240 m a.s.l.) in  
1026 the Bolivian Andes, *Atmospheric Chemistry and Physics*, 23, 4559-4576, 10.5194/acp-23-4559-2023,  
1027 2023a.

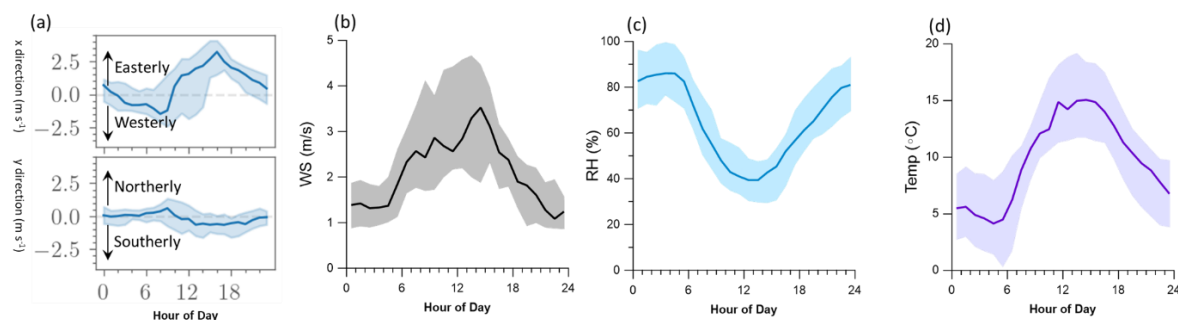
1028 Zha, Q., Yan, C., Junninen, H., Riva, M., Sarnela, N., Aalto, J., Quéléver, L., Schallhart, S., Dada, L.,  
1029 Heikkinen, L., Peräkylä, O., Zou, J., Rose, C., Wang, Y., Mammarella, I., Katul, G., Vesala, T., Worsnop,  
1030 D. R., Kulmala, M., Petäjä, T., Bianchi, F., and Ehn, M.: Vertical characterization of highly oxygenated  
1031 molecules (HOMs) below and above a boreal forest canopy, *Atmospheric Chemistry and Physics*, 18,  
1032 17437-17450, 10.5194/acp-18-17437-2018, 2018.

1033 Zha, Q., Aliaga, D., Krejci, R., Sinclair, V., Wu, C., Ciarelli, G., Scholz, W., Heikkinen, L., Partoll, E.,  
1034 Gramlich, Y., Huang, W., Leiminger, M., Enroth, J., Peräkylä, O., Cai, R., Chen, X., Koenig, A. M.,  
1035 Velarde, F., Moreno, I., Petäjä, T., Artaxo, P., Laj, P., Hansel, A., Carbone, S., Kulmala, M., Andrade,  
1036 M., Worsnop, D., Mohr, C., and Bianchi, F.: Oxidized organic molecules in the tropical free  
1037 troposphere over Amazonia, *National Science Review*, 10.1093/nsr/nwad138, 2023b.

1038 Zheng, Y., Chen, Q., Cheng, X., Mohr, C., Cai, J., Huang, W., Shrivastava, M., Ye, P., Fu, P., Shi, X., Ge,  
1039 Y., Liao, K., Miao, R., Qiu, X., Koenig, T. K., and Chen, S.: Precursors and Pathways Leading to  
1040 Enhanced Secondary Organic Aerosol Formation during Severe Haze Episodes, *Environ Sci Technol*,  
1041 55, 15680-15693, 10.1021/acs.est.1c04255, 2021.

1042

1043

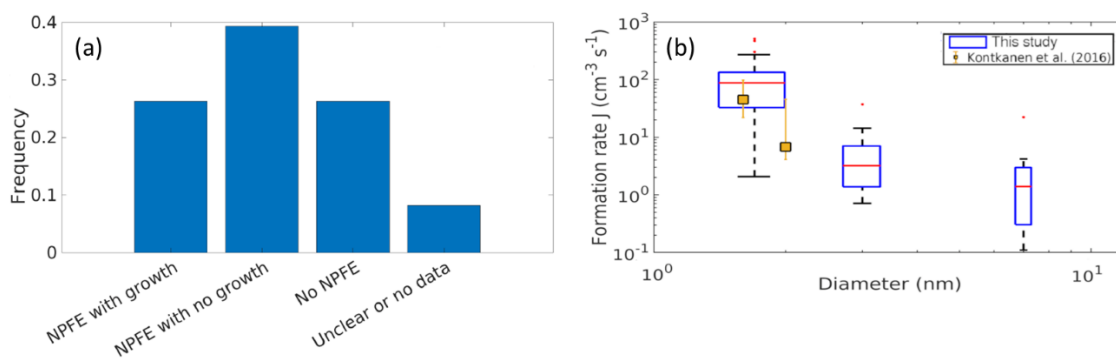


1044

1045 **Figure 1.** The diurnal variations of (a) average wind vectors, (b) wind speed, (c) relative humidity (RH), and (d)  
1046 temperature.

1047

1048

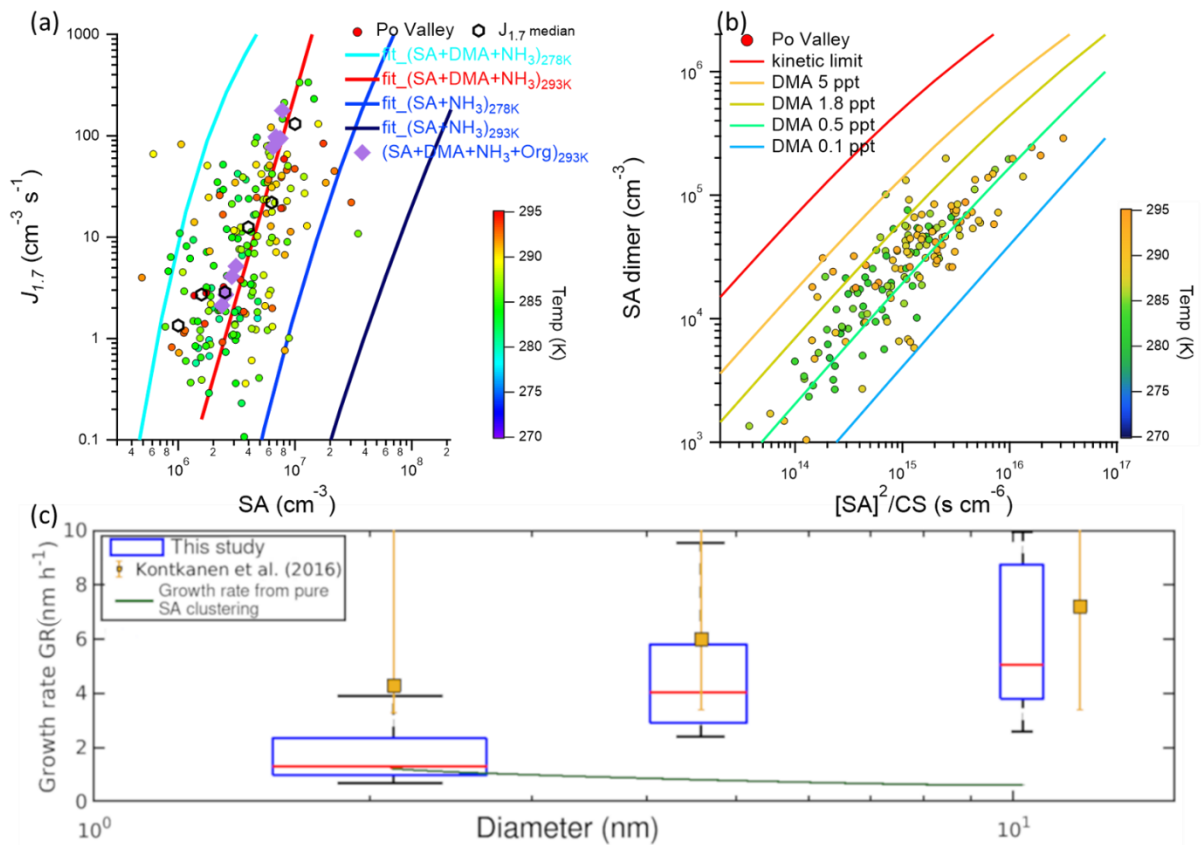


1049

1050 **Figure 2.** (a) The frequency of NPF events with and without growth, of days without NPF, and days with unclear  
1051 classification or no data during this study, (b) calculated formation rates at 1.7 nm, 3 nm and 7 nm from this  
1052 study and values reported by Kontkanen et al. 2016 (yellow squares). The red lines are the median values of the  
1053 maximum formation rates measured during an NPF event, the blue boxes show the values between 25th and 75th  
1054 percentiles and the black whiskers mark the 5<sup>th</sup> and 95<sup>th</sup> percentiles. Red dots are outliers, and the width of the  
1055 box is proportional to the square root of the number of the  $J$  values.

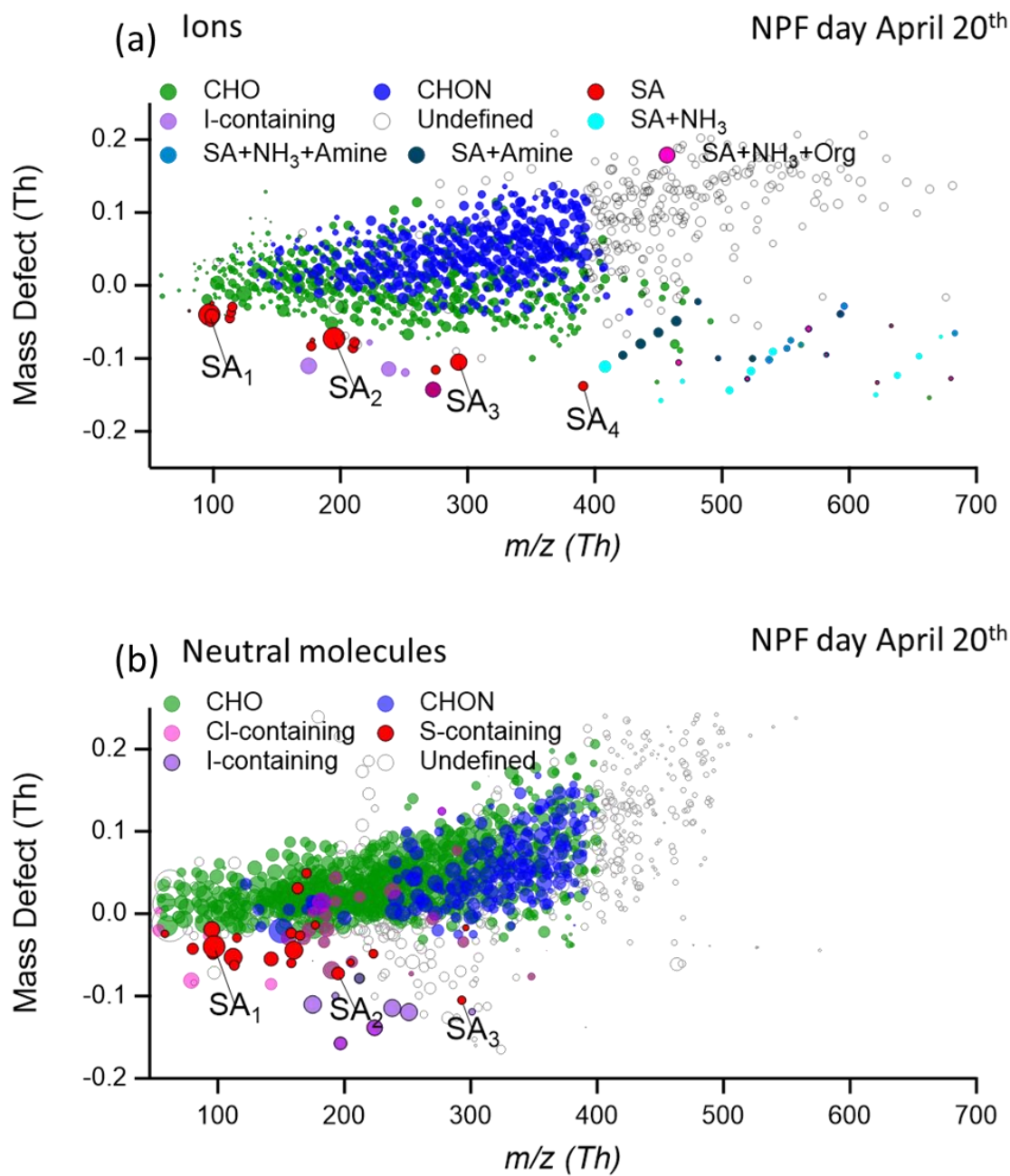
1056





1057

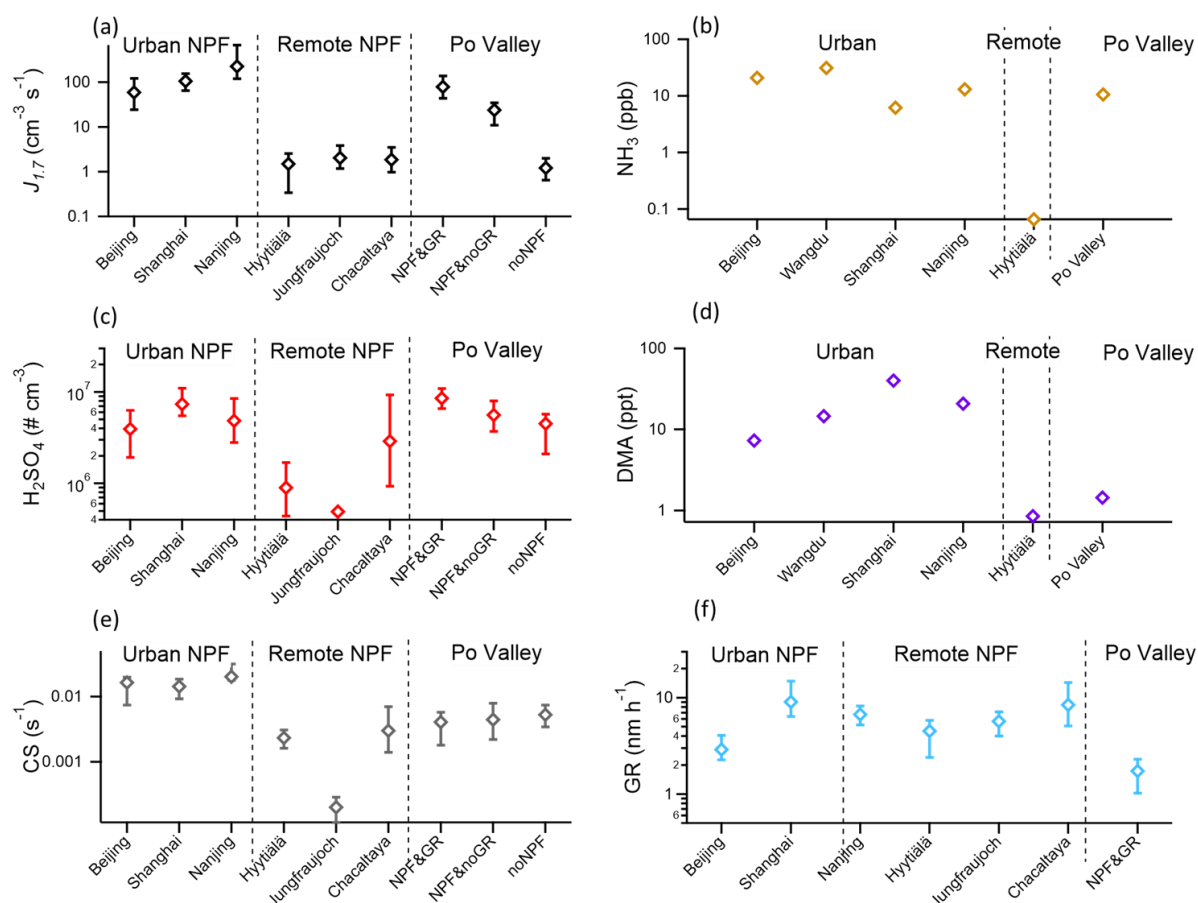
1058 **Figure 3.** (a) The formation rate of 1.7 nm particles ( $J_{1.7}$ ) versus SA concentrations in during springtime in the Po  
 1059 Valley (shown as circles) and experimental results from CLOUD chamber experiments (shown as solid diamonds).  
 1060 The solid lines are from fitted results of CLOUD chamber experiments and the black hexagon represented the  
 1061 mean values under different SA levels, (b) the relationship between sulfuric acid dimer concentration (SA dimer),  
 1062 the square of monomer concentrations (SA)<sup>2</sup>, and the CS. The lines are from the kinetic model simulations under  
 1063 different DMA levels and the dots are from the measurement. In (a) and (b), the results from the field  
 1064 measurements are from the daytime (10:00 – 14:00 LT) and color-coded by the temperature at the site. The  $J_{1.7}$   
 1065 and corresponding SA concentrations of CLOUD chamber results are from previous literature (Xiao et al., 2021).  
 1066 (c) Calculated growth rates for 1.5 – 3 nm, 3 – 7 nm, and 7 – 15 nm from this study and values reported by  
 1067 Kontkanen et al. (2016, yellow squares). The red horizontal lines are the median values, the blue boxes show the  
 1068 values between 25<sup>th</sup> and 75<sup>th</sup> percentiles and the black whiskers mark the 5<sup>th</sup> and 95<sup>th</sup> percentiles. The green solid  
 1069 line represents predicted growth rates from pure sulfuric acid without organics condensation (Stolzenburg et al.,  
 1070 2020). The width of the box is proportional to the square root of the number of the GR values.



1071

1072 **Figure 4.** Mass defect plots, which represent the difference between compounds' exact mass and nominal mass,  
 1073 for (a) ion clusters and (b) neutral clusters during the NPF period (10:00 – 14:00 LT) of April 20. The size of the  
 1074 dots is proportional to the logarithm of the signal intensity of each cluster.

1075



1076

1077 **Figure 5.** Parameters and gaseous precursors of NPF in the Po Valley and other environments. (a) formation rate  
 1078 of sub-2 nm particles, (b) the atmospheric  $\text{NH}_3$  concentrations, (c) SA concentrations, (d) DMA concentrations,  
 1079 (e) CS levels, and (f) growth rate in different environments. The diamond dots represent the median values, and  
 1080 the error bars represent the 25<sup>th</sup> and 75<sup>th</sup> percentiles. For the Po Valley data, the formation rates, growth rates, SA  
 1081 concentrations and CS data were selected for 10:00 – 14:00 LT. The formation rates, growth rates, SA  
 1082 concentrations and CS during NPF in Beijing, Shanghai, Hyvitiälä, Jungfraujoch and Chacaltaya are from Deng  
 1083 et al. (2020). The GR calculation range varies for different sites. Beijing ( $\text{GR}_{7-15}$ , (Deng et al., 2020)), Shanghai  
 1084 ( $\text{GR}_{7-25}$ , (Yao et al., 2018)), Nanjing ( $\text{GR}_{3-20}$ , (Yu et al., 2016)), Hyvitiälä ( $\text{GR}_{3-20}$ , (Vana et al., 2016)),  
 1085 Jungfraujoch ( $\text{GR}_{7-20}$ , (Boulon et al., 2010)), Chacaltaya ( $\text{GR}_{7-20}$ , (Rose et al., 2015)), and Po Valley ( $\text{GR}_{7-15}$ , this  
 1086 study) are used for comparison. The  $\text{NH}_3$  and DMA concentrations are from literature, which is listed in the Table  
 1087 S1. Half of the limit of detection (LOD) of DMA concentrations in Hyvitiälä was applied in panel d. DMA  
 1088 concentrations in Po Valley was not presented since it is not quantified in this study.